RESEARCH ARTICLE | MARCH 02 2026

Cross Sections for Electron Collisions with Molecular and Atomic Oxygen FREE

Mi-Young Song ; Hyuck Cho; Grzegorz P. Karwasz ; Viatcheslav Kokoouline ; Jonathan Tennyson ; Klaus Bartschat

J. Phys. Chem. Ref. Data 55, 013102 (2026)
https://doi.org/10.1063/5.0287254

Journal of Physical and Chemical Reference Data ARTICLE pubs.aip.org/aip/jpr

Cross Sections for Electron Collisions with Molecular and Atomic Oxygen

Cite as: J. Phys. Chem. Ref. Data 55, 013102 (2026); doi: 10.1063/5.0287254
Submitted: 24 June 2025 • Accepted: 10 December 2025 •
Published Online: 2 March 2026

Mi-Young Song,[1,a)] Hyuck Cho,[2] Grzegorz P. Karwasz,[3] Viatcheslav Kokoouline,[4] Jonathan Tennyson,[5] and Klaus Bartschat[6]

AFFILIATIONS

[1] Institute of Plasma Technology, Korea Institute of Fusion Energy(KFE), 37, Dongjangsan-ro, Gunsan, Jeollabuk-do 54004, South Korea
[2] Department of Physics, Chungnam National University, Daejeon 34134, South Korea
[3] Institute of Physics, Astronomy and Applied Informatics, Nicolaus Copernicus University, Grudziadzka 5, 87-100 Toruń, Poland
[4] Department of Physics, University of Central Florida, Orlando, Florida 32816, USA
[5] Department of Physics and Astronomy, University College London, Gower Street, London WC1E 6BT, United Kingdom
[6] Department of Physics and Astronomy, Drake University, 2507 University Ave, Des Moines, Iowa 50311, USA

[a)] **Author to whom correspondence should be addressed:** mysong@kfe.re.kr

ABSTRACT

Electron collision cross section data are compiled from the literature for electron collisions with the oxygen molecule O_2 and the atom O. Cross sections are collected and reviewed for total scattering, elastic scattering, momentum transfer, rotational excitation, vibrational excitation, electronic excitation, dissociative processes, and ionization. The literature has been surveyed up to the end of 2024. For each of these processes, the recommended values of the cross sections are presented with an estimated uncertainty.

Published by AIP Publishing on behalf of the National Institute of Standards and Technology. https://doi.org/10.1063/5.0287254

CONTENTS

List of Tables

List of Figures

1. Introduction

Earth, the blue planet as seen by Apollo astronauts, would not appear blue without oxygen in the atmosphere. In fact, James Lovelock, when asked by NASA in the 1970s if there were life on Mars, answered "No," on the basis of the color of the atmosphere of the Red Planet. Oxygen in the Earth's atmosphere is a "by-product," which results from the first billion years of life.

Both atomic oxygen, O, and molecular oxygen, O_2, are open-shell species with triplet ground states: ^3P and $^3\Sigma_g^-$, respectively. This distinguishes molecular oxygen from other diatomic atmospheric molecules.

Peculiar features of the O_2 molecule include low thresholds for excitation to the singlet electronic states $a^1\Delta_g$ and $b\,^1\Sigma_g^+$ at 0.98 and 1.63 eV, respectively, and also for the spin-allowed but symmetry-forbidden $^3\Sigma_u^+$ state (the Herzberg system at 6.47 eV). Furthermore, a low threshold for the dissociation into neutrals (5.12 eV) makes both the O_2 molecule and the O atom the species that determine the radiation budget and the Earth's atmospheric chemistry. The Sun's spectrum predominantly contains wavelengths from 160 to 3000 nm (0.41–7.75 eV) with 97.9% irradiance falling in this range:[1] oxygen species, including ozone (O_3), contribute significantly to the harvesting of solar power flux. The human eye is sensitive to wavelengths longer than 380 nm, where there is an abrupt fall in absorption by O_3, see Ref. 2, and shorter than 760 nm, i.e., where the A-band of the O_2 molecule starts. Hence, oxygen defines the visible range of sunlight due to absorption in the Earth's troposphere.[3]

One interesting application of the particular features of molecular oxygen is its use in the optical treatment of melanoma.[4] Here, a pharmachemical containing a photosensitizer, designed to accumulate in the tumor tissue, is supplied to the patient. Then, the tumor is illuminated with infrared (IR) light, causing electronic excitation of the O_2 molecule to a metastable singlet state. Singlet O_2 is

highly reactive and its creation leads to the internal burning of the tumor.[5,6]

The cross section for oxygen molecules due to electron impact is an important parameter in plasma science and engineering, affecting the fundamental processes that govern plasma conditions. Ionization, dissociation, and excitation reactions contribute to the production of reactive oxygen species (ROS), particularly electrons, atoms, and ions, which directly affect the applications of plasma in various fields. Given the critical role that oxygen plasma plays in key technologies, including semiconductor etching, spacecraft propulsion, plasma medicine,[7] and environmental applications,[8] there is a need to improve our understanding of electron impact cross sections.

There have been a number of compilations of electron collision cross sections for oxygen. Itikawa and co-workers[9,10] dedicated their review papers to total and partial cross sections of the O_2 molecule; Zecca, Karwasz, and Brusa,[11] Brunger and Buckman,[12] and Anzai *et al.*[13] compared O_2 cross sections with some other molecules; the Landolt-Börnstein compilation gives recommended total,[14] elastic,[15] momentum transfer,[16] and ionization[17] cross sections. Itikawa and Ichimura[18] reviewed total and partial cross sections for atomic oxygen, while Laher and Gilmore[19] reviewed its ionization and electronic excitation cross sections.

The review by Itikawa[10] remains a standard reference for modeling electron diffusion processes in oxygen.[20] However, since that review new, accurate measurements of O_2 total cross sections (TCS) at very low energies, where sharp resonant structures appear, have been made, and substantial progress has also been achieved in theoretical methods. The latter now enable calculations of not only elastic scattering, but also vibrational and electronic excitation cross sections, both for the molecule and the oxygen atom, including their metastable species.

The present review covers the bibliography up to the end of 2024.

2. O_2 Molecule

2.1. Total scattering cross section

TCS are usually measured by employing de Beer's attenuation method. This approach requires only the target gas pressure and the electron currents to be monitored. Hence, the potential accuracy of the measured TCS is high, about 5%–10%. Details of experimental techniques have been outlined in our previous review on electron collisions with methane.[21] However, in the case of O_2 we find somewhat larger discrepancies between data from different laboratories (cf. Fig. 1) than was the case, for example, for CH_4; see Ref. 21.

At low energies, Salop and Nakano[22] applied Ramsauer's method (i.e., a perpendicular magnetic field as the energy selector); Subramanian and Kumar[23] used a photoelectron source (UV photons produced from a microwave discharge in noble gases) and an electrostatic mirror energy analyzer. Measurements referred to as Zecca *et al.*[24] were obtained in two laboratories: in Trento with an "aperture" energy monochromator and retarding field analyzer and in Gdańsk with a cylindrical electrostatic monochromator. The energy resolution in both experiments was similar, about 70 meV. The "Gdańsk" apparatus was also used by Szmytkowski, Maciag, and Karwasz.[25] Kanik, Nickel, and Trajmar[26] measured the TCS in the energy range 5–300 eV using a linear transmission method. A rather long (144 mm) scattering cell assured good angular resolution; the declared systematic errors were within 2%.

The agreement with older experiments, like that by Salop and Nakano,[22] is particularly poor in the few eV region. The main reason is, probably, the lack of adequate analyzers for the inelastically scattered electrons: this effect tends to underestimate the TCS. Also, Subramanian and Kumar's[23] cross sections are lower than the majority of other results in the region 2–5 eV. A similar discrepancy with results from that laboratory was observed for noble gases.[27] A probable reason is the complexity of the normalization

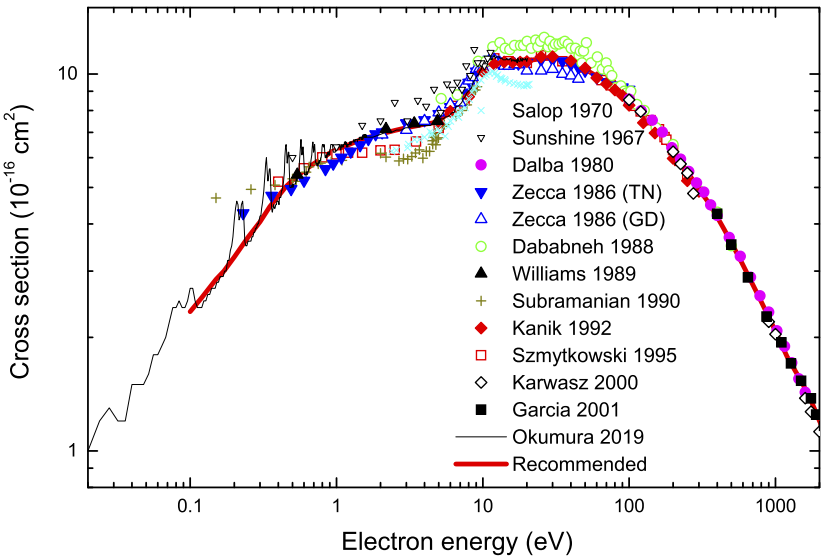

FIG. 1. Comparison of experimental TCS for electron scattering on O_2: black inverted triangles;[28] cyan x;[22] pink circles: high-energy data from the Trento lab;[29] blue inverted triangles: low-energy data from the Trento lab;[24] blue open triangles: Gdańsk lab;[24] green open circles;[30] red diamonds;[26] red open squares;[25] black open diamonds: improved high-energy data from the Trento lab;[14] black squares;[31] thin black line.[32] The thick red line represents our recommended values. For the TCS in the very-low energy range, see Fig. 2.

procedures required for the photoelectron source. Early data by Sunshine, Aubrey, and Bederson[28] were obtained using the molecular-beam recoil method and differ by about +10% from other experiments. Note that the recoil method was used predominantly for "exotic" (and highly polar) targets, like metal halides.[14]

The TCS by Dababneh *et al.*[30] were obtained using an apparatus designed for both positron and electron scattering, with a long scattering cell (109 cm) and a weak guiding magnetic field. Corrections were estimated for forward scattering. These data are somewhat higher than other sets in the energy range 10–100 eV. In the high-energy range, there are measurements from two laboratories, Trento University - earlier by Dalba *et al.*[29] and newer, with an improved angular resolution by Karwasz, Brusa, and Zecca,[14] and from Madrid University by García, Blanco, and Williart;[31] only the latter measurements[31] were obtained using a retarding field analyzer and hence are more reliable.

The very-low-energy electron scattering on the O_2 molecule is characterized by the $^2\Pi_g$ resonance, which is clearly visible as a vibrational-like structure in the TCS. We compare measurements in the 0–1.5 eV energy range in Fig. 2. Field and collaborators[33,34] used synchrotron radiation as the source of photoelectrons and a longitudinal focusing magnetic field. The energy resolution of their apparatus was 3 meV. They reported, respectively, the signal of scattered electrons into the 60°–120° angular range[33] and the cross sections for the backward hemisphere (90°–180°) in the 10–175 meV range.[34] Extrapolating the scattering length from the backward scattering result, they obtained 0.34×10^{-16} cm^2 for the TCS. The absolute TCS from the Canberra time-of-flight apparatus[35] and the Tokyo synchrotron-based measurements[32] agree reasonably well, both in the magnitude and the positions of the resonant peaks.

The recommended TCS values are given in Table 1. In the very-low energy range (0.1–1eV), they are based on the nonresonant background values from Okumura *et al.*,[32] between 1 and 100 eV on the absolute TCSs of Refs. 24–26, above 100 eV on Refs. 26, 29, and 31. The uncertainty in the recommended TCS is 5%–10%. The detailed TCS in the very-low-energy range, from the experiment by Okumura *et al.*,[32] is given in Table 2.

Somewhat surprisingly (as the two experimental methodologies are quite distinct), the presently recommended TCS (based on the most recent measurements) agree within 5% with the recommended integral elastic cross sections; see Table 4. The agreement is almost perfect up to 4 eV, i.e., at energies below where electronic excitations are significant.

TABLE 1. Recommended TCS for O_2. The uncertainty below 1.0 eV is about 10%, between 1 and 500 eV about 5%, and 7% above 500 eV

Electron energy (eV)	Total cross section (10^{-16} cm^2)	Electron energy (eV)	Total cross section (10^{-16} cm^2)
0.1	2.34	11	10.7
0.2	3.27	12	10.8
0.3	4.05	15	10.7
0.4	4.74	20	10.8
0.5	5.22	25	10.97
0.6	5.54	30	11.0
0.7	5.78	40	10.8
0.8	5.97	50	10.3
0.9	6.17	60	9.87
1.0	6.30	70	9.52
1.2	6.48	80	9.23
1.5	6.72	90	8.98
2.0	6.93	100	8.68
2.5	7.08	120	7.97
3.0	7.20	150	7.21
3.5	7.28	200	6.24
4.0	7.36	250	5.51
4.5	7.41	300	4.94
5.0	7.52	400	4.17
6.0	7.93	500	3.58
7.0	8.39	600	3.11
8.0	9.16	700	2.76
9.0	9.90	800	2.49
10.0	10.4	1000	2.08

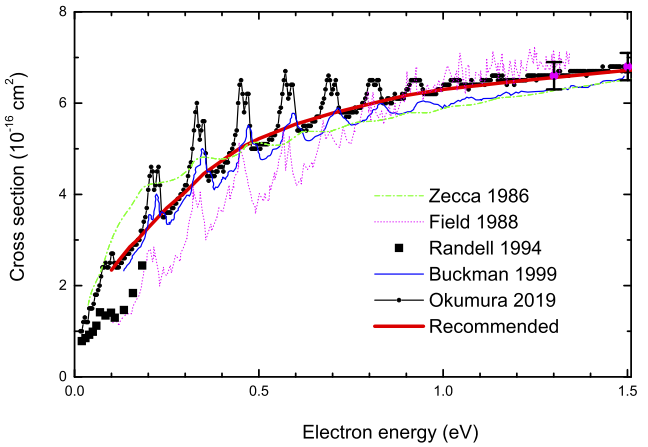

FIG. 2. Experimental TCS for electron scattering from O_2 in the very-low-energy range: green dash-dotted line: absolute TCS from the Trento lab;[24] magenta dotted-line: signal of scattered electrons into the 60°–120° angular range,[33] normalized to the present recommended TCS at 1 eV; black squares: backward scattering cross section;[34] blue line: absolute TCS from the Canberra lab;[35] black points and line: Tokyo absolute TCS.[32] At 1.3 and 1.5 eV, we show the total error bars. The thick red line is our recommended TCS. Apart from the TCS of Okumura *et al.*,[32] all other data are digitized from the figures in the papers.

2.2. Elastic scattering cross section

Experimental studies of the elastic angle-differential cross section (DCS) and the integral cross section (ICS) for electron scattering with molecular oxygen are much more abundant than for atomic oxygen. There have been many reports on measurements of the elastic DCSs and ICSs. Here we focus on those results that are important for our recommendations. Shyn and Sharp[36] performed experiments in the 2–200 eV energy range extending them to larger scattering angles than other researchers normally did. However, their cross sections generally proved to be a little larger than other measured cross section at energies around 10 eV and below for most molecules they studied, including molecular oxygen. Iga *et al.*[37]

TABLE 2. Recommended TCS for O_2 in the very-low-energy range from the experiment by Okumura *et al.*[32] The uncertainties are within $\pm 0.2 \times 10^{-16}$ cm^2

Electron energy (eV)	Total cross section (10^{-16} cm^2)	Electron energy (eV)	Total cross section (10^{-16} cm^2)
0.016	1.0	0.801	6.5
0.020	1.0	0.861	6.0
0.024	1.2	0.921	6.5
0.032	1.2	1.001	6.4
0.040	1.5	1.101	6.4
0.060	1.8	1.301	6.6
0.080	2.4	1.501	6.8
0.100	2.7	1.771	6.8
0.120	2.4	2.171	7.0
0.140	2.7	2.571	7.1
0.160	2.9	2.971	7.2
0.180	3.2	3.971	7.3
0.200	4.2	4.971	7.5
0.220	4.2	5.971	7.8
0.240	3.5	6.971	8.3
0.260	3.6	7.971	9.0
0.300	4.2	8.971	9.8
0.340	5.2	9.971	10.6
0.380	4.4	10.971	10.9
0.420	4.9	11.971	11.2
0.460	5.8	12.971	11.1
0.500	5.1	13.971	10.9
0.540	5.3	14.971	10.9
0.580	6.1	15.971	10.9
0.621	5.5	16.971	10.9
0.661	5.7	17.971	10.8
0.701	6.3	18.971	10.9
0.741	5.8	19.971	10.8

reported cross sections for 300–1000 eV, while Sullivan *et al.*[38] conducted their experiment at the lower energy range of 1–30 eV. Green *et al.*[39] repeated the same measurement at 5, 7, and 10 eV to confirm the results of Sullivan *et al.* Later, Linert, King, and Zubek[40] measured the cross sections near backward scattering angles using an angle-changing device for the energy region of 7–20 eV. For our recommended DCSs, we mostly rely on Sullivan *et al.*[38] combined with, if available, Linert, King, and Zubek[40] at backward angles. The DCS uncertainties vary between 7% and 10% depending on the electron energies and the angular ranges. The recommended DCSs are presented in Fig. 3 for four representative electron energies. The entire set of recommended DCSs is given in Table 3.

The elastic ICS are derived from the DCSs by integrating them over all scattering angles. For the forward and backward scattering angles, where experimental DCSs are generally not available, extrapolation techniques are used that will not be described here. There are several previous reviews on the elastic ICSs of electron scattering with molecular oxygen: Buckman, Brunger, and Elford[15] recommended ICSs for the energy region of 1–100 eV using the DCSs from several groups, while Itikawa[10] followed the recommendation of

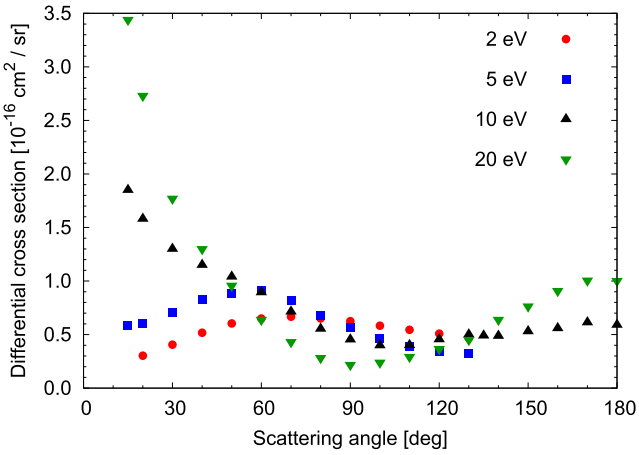

FIG. 3. Recommended DCSs for O_2 for representative incident electron energies. The uncertainties vary between 7% and 10% depending on the electron energies and the angles.

Buckman, Brunger, and Elford[15] with an extension to 100–1000 eV using the data of Kanik, Trajmar, and Nickel.[41]

For our recommendation, we compiled the previously reported elastic ICSs from the literature cited in the discussion of the elastic DCSs above. Since we recommend Sullivan *et al.*[38] and Linert,

TABLE 3. Recommended DCS of O_2 (in 10^{-16} cm^2 sr^{-1}). The uncertainties vary between 7% and 10% depending on the electron energies and the angles

Angle (deg)	2.0 eV DCS	3.0 eV DCS	5.0 eV DCS	7 eV DCS	10 eV DCS	15 eV DCS	20 eV DCS	30 eV DCS
12						3.03		
15			0.585	0.877	1.85	2.76	3.44	5.08
20	0.303	0.418	0.603	0.836	1.58	2.29	2.73	3.84
30	0.406	0.552	0.706	0.853	1.30	1.71	1.77	2.02
40	0.517	0.644	0.824	0.910	1.15	1.38	1.30	1.11
50	0.604	0.728	0.886	0.931	1.04	1.11	0.958	0.654
60	0.650	0.770	0.914	0.881	0.894	0.844	0.639	0.420
70	0.667	0.743	0.815	0.780	0.714	0.599	0.431	0.270
80	0.651	0.685	0.677	0.620	0.554	0.423	0.282	0.184
90	0.625	0.605	0.565	0.500	0.453	0.333	0.218	0.137
100	0.583	0.536	0.464	0.421	0.399	0.298	0.239	0.130
110	0.544	0.470	0.391	0.371	0.401	0.304	0.293	0.166
120	0.509	0.424	0.343	0.369	0.455	0.409	0.367	0.257
130	0.468	0.386	0.323	0.401	0.500	0.468	0.452	
132								0.390
135				0.408	0.490			
140				0.433	0.487	0.588	0.639	
144								0.666
150				0.464	0.53	0.647	0.764	
160				0.473	0.559	0.727	0.908	
170				0.478	0.613	0.812	1.005	
180				0.474	0.590	0.819	1.002	

King, and Zubek[40] for the DCSs, we use them again for our recommended ICSs in the low energy (1–20 eV) range. The ICSs of Shyn and Sharp[36] are too high in the 2–10 eV energy range; however, from 40-200 eV, there are no ICSs reported except for those of Shyn and Sharp.[36] Their measurements are generally accepted as reliable in the energy region above 10 eV. Furthermore, at 20 and 30 eV, the measurements of Sullivan *et al.*[38] and Shyn and Sharp[36] match reasonably well. Therefore, we recommend Shyn and Sharp's ICS in the 40–200 eV energy region.

In the higher energy range, Shyn and Sharp's ICSs do not match smoothly with those of Iga *et al.*[37] who reported ICSs for 300–1000 eV. Daimon *et al.*[42] also derived ICSs for 200–500 eV; these three ICS sets for the 200–1000 eV region come from different laboratories and show some disagreement with each other. Kanik and Trajmar[41] combined the ICS/DCSs of Shyn and Sharp,[36] Iga *et al.*,[37] and Daimon *et al.*[42] to derive the ICS in the high energy (200–1000 eV) region, and the result matches the ICSs of Shyn and Sharp at 200 eV.

In summary, we use Sullivan *et al.*[38] from 1 to 20 eV, Shyn and Sharp[36] for 20–200 eV, and Kanik and Trajmar[41] with Iga *et al.*[37] for 200–1000 eV to form our recommendation of the elastic ICSs. The uncertainty of the ICSs below 10 eV is about 20%, and from around 10–1000 eV about 10%–15%. The recommended results are presented in Fig. 4 and Table 4.

2.3. Momentum transfer cross section

There have been several previous reviews on the elastic momentum transfer cross sections (MTCSs) of electron scattering with oxygen molecules. Elford, Buckman, and Brunger [16] recommended MTCS in the low-energy range (<0.3 eV) based on the analysis of electron transport coefficient data provided by Yousfi (1987) through "personal communication." See "87You1" in references for Sec. 6.3.5.6 of Ref. 16. At energies above 0.6 eV, Elford, Buckman, and Brunger[16] preferred the cross section derived by Itikawa *et al.*[9] from beam data. Later, Itikawa[10] updated the recommended MTCS by modifying them with the DCSs of Linert, King, and Zubek,[40] but the contribution of the "personal communication" component, which originated from Elford, Buckman, and Brunger,[16] was still retained in the low-energy range.

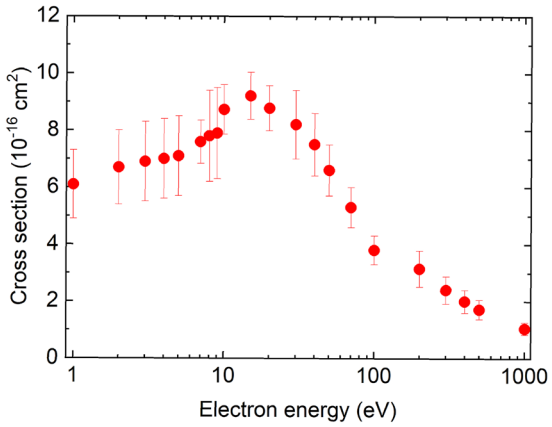

FIG. 4. Recommended elastic ICS for O_2.

TABLE 4. Recommended elastic ICS for O_2. The uncertainty below 10 eV is about 20%, and above 10 eV about 10%–15%

Electron energy (eV)	ICS (10^{-16} cm^2)
1	6.10
2	6.70
3	6.90
4	7.00
5	7.10
7	7.59
8	7.89
9	7.99
10	8.73
15	9.21
20	8.73
30	8.20
40	7.50
50	6.60
70	5.30
100	3.80
200	3.15
300	2.40
400	2.00
500	1.72
1000	1.05

Our policy in recommendation is that we compile and use only data published in peer-reviewed journals. Following this policy, the recommendation of Elford, Buckman, and Brunger[16] based on a private communication is not acceptable. The MTCS values are derived in two ways: for energies above 1 eV, they are derived from integrated DCSs similar to the derivation of ICSs, while in the very-low-energy region (<1 eV), they are derived from swarm experiments. In the energy region from 1 to 200 eV, for the same reason as for the ICS case, we recommend the MTCS derived from Sullivan *et al.*,[38] Linert, King, and Zubek,[40] Shyn and Sharp.[36] For 300–1000 eV Iga *et al.*[37] reported MTCS values. Here Iga *et al.* and Shyn and Sharp match quite smoothly. Therefore, in the high-energy region, we recommend these DCS-derived MTCS. At low energies, a few swarm measurements have been reported. Itikawa showed some of them, for example by Hake and Phelps,[43] in his old review.[44] But the swarm data are quite scattered and not consistent. In 2003, Jeon[45] published extensive electron collision cross sections including the MTCSs for the oxygen molecule obtained from an electron swarm study, but they did not provide uncertainty estimates. We take these MTCSs for 0.001 eV up to 0.8 eV and, together with the beam data and recommend values for the MTCS from 0.001 to 1000 eV. The uncertainties of the MTCSs are about 20% from 1 to 10 eV and about 10%–15% from 10 to 1000 eV. The recommended results are presented in Fig. 5 and Table 5.

2.4. Rotational excitation cross section

In its ground electronic state X $^3\Sigma_g^-$, the main isotopologue $^{16}O_2$ (as well as the $^{18}O_2$ isotopologue) can have only odd values of the nuclear rotation angular-momentum quantum number, N.

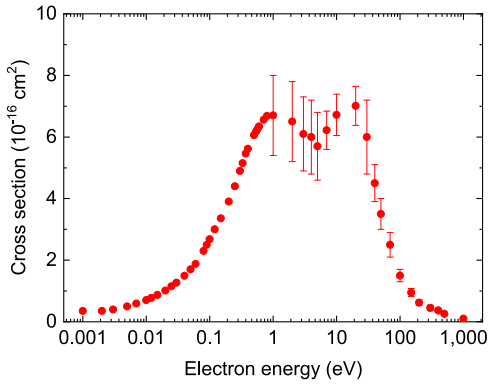

FIG. 5. Recommended elastic MTCS for O_2. The uncertainties from 1 to 10 eV are about 20%, and from 10 to 1000 eV about 10%–15%.

There are no experimental or accurate theoretical data available on rotational excitation of O_2. The previous reviews Itikawa,[10] Tanaka *et al.*,[46] and Alves *et al.*[47] recommended using cross sections obtained with the Born approximation for electron impact rotational excitation from N to $N \pm 2$. Specifically,[48]

$$\sigma_{N' \leftarrow N}(E_{el}) = \frac{8\pi Q_v^2}{15 a_0^2} c_{N',N}, \quad (1)$$

where a_0 is the Bohr radius. The coefficients $c_{N',N}$ are nonzero only for $N' = N \pm 2$, i.e.,

$$c_{N+2,N} = \frac{(N+1)(N+2)}{(2N+1)(2N+3)} \sqrt{1 - \frac{B_v(4N+6)}{E_{in}}},$$

$$c_{N-2,N} = \frac{N(N-1)}{(2N-1)(2N+1)} \sqrt{1 + \frac{B_v(4N-2)}{E_{in}}},$$

where B_v and Q_v are the rotational constant and the quandrupole moment of the vibrational level, respectively, and E_{el} is the energy of the incident electron. For the lowest vibrational levels of O_2 in its ground electronic state, one can use the experimental values $B_0 = 1.792 \times 10^{-4}$ eV and $Q_0 = -0.230\ a_0^2$ obtained[49,50] for the ground vibrational level $v = 0$ of O_2 ($X\ ^3\Sigma_g^-$).

This approximation shows that the rotational excitation cross section is small compared to that of molecules with permanent dipole moments. However, detailed results should be used with caution because the approximation neglects the important fine-structure effects arising from the coupling of the electron spin with the rotational motion.[51] Previous studies on electron impact rotational excitation suggested that short-range interactions dominate over long-range quadrupole effects for molecules without a permanent dipole moment.[52]

TABLE 5. Recommended elastic MTCS for O_2. The uncertainties from 1 to 10 eV are about 20%, and from 10 to 1000 eV about 10%–15%. Below 1 eV, Jeon[45] did not provide uncertainties for their MTCS

Electron energy (eV)	MTCS (10^{-16} cm^2)	Electron energy (eV)	MTCS (10^{-16} cm^2)
0.001	0.35	0.50	6.06
0.002	0.35	0.54	6.18
0.003	0.40	0.57	6.26
0.005	0.50	0.60	6.34
0.007	0.59	0.71	6.56
0.010	0.70	0.80	6.68
0.012	0.77	1.0	6.70
0.015	0.87	2.0	6.50
0.020	1.01	3.0	6.10
0.025	1.15	4.0	6.00
0.030	1.27	5.0	5.70
0.040	1.49	7.0	6.22
0.050	1.70	10	6.72
0.060	1.88	20	7.01
0.008	2.30	30	6.00
0.090	2.50	40	4.50
0.10	2.68	50	3.50
0.12	3.00	70	2.50
0.15	3.36	100	1.50
0.20	3.90	150	0.95
0.25	4.40	200	0.62
0.30	4.90	300	0.45
0.33	5.15	400	0.37
0.37	5.46	500	0.26
0.40	5.62	1000	0.10

2.5. Vibrational excitation cross section

Vibrational excitation of O_2 in its ground electronic state $X\ ^3\Sigma_g^-$ is strongly influenced by the $O_2^-\ ^2\Pi_g$ resonant state,[53,54] situated ~0.4 eV above the $X\ ^3\Sigma_g^-$ state. The resonance appears also in the total and elastic cross sections at energies below 1 eV (see Figs. 1 and 2) with a clearly seen vibrational structure. The vibrational levels in that resonant state produce resonances in the e-O_2 spectra, spaced by ~0.1 eV. In low-resolution experiments (such as those by Shyn and Sweeney[55]), one observes a single feature, the electronic resonance. Another resonance is situated around 10 eV above the ground state of O_2. It corresponds to several purely dissociative electronic resonances[56] of O_2^- and, therefore, does not have a fine vibrational structure at high resolution.

Cross sections for vibrational excitation have been measured since 1971 by Allan,[53] Linder and Schmidt,[57] Wong, Boness, and Schulz,[58] Noble *et al.*,[59] Brunger, Middleton, and Teubner,[60] and Linert and Zubek.[61] There have been several theoretical studies for determining the cross sections, in particular by Laporta, Celiberto, and Tennyson,[54] Noble *et al.*,[59] Higgins *et al.*,[62] and Alt and Houfek.[63]

In the previous review by Itikawa[10] (the same data were recommended in a later review[46]), for energies below 1 eV, i.e., in the region where the $^2\Pi_g$ resonance influences the vibrational excitation process, cross sections derived from the measurements by Allan[53] were recommended, while the recommended cross sections at higher energies were based on the results by Shyn and Sweeney,[55] except for the $v = 0 \rightarrow v' = 1$ transition at 10 eV, for which the cross section by Linert and Zubek[61] was recommended.

Since the two last reviews,[10,46] two theoretical studies were published. Laporta, Celiberto, and Tennyson[54] used an R-matrix

approach to find energies and widths of electronic resonances as a function of internuclear separation, and the vibrational motion was accounted for in the excitation process using the boomerang model. Cross sections for vibrational excitation transitions between all 42 vibrational levels of O_2 were computed. Later, Alt and Houfek[63] used the UK molecular R-matrix code[64] and a nonlocal resonance model for vibrational motion in the theory of electron-molecule scattering, accounting for the spin-orbit coupling. They presented computed cross sections for seven transitions $v = 0 \rightarrow v' = 1 - 7$.

The results of the two recent theoretical studies agree well for the energies of vibrational resonances, but the cross sections for certain transitions differ by as much as a factor of 4. The nonlocal resonance model, employed by Alt and Houfek,[63] is known to be very sensitive—more than the boomerang model of Ref. 54—to accurate energies of the electronic resonances. The results by Laporta, Celiberto, and Tennyson[54] agree better with the measurements.[53,59] Therefore, we recommend the theoretical data of Ref. 54, apart from the non-resonance part (1–8 eV and above 12 eV) of the 0–1 transition where the experiment data by Noble *et al.*[59] are more appropriate. The uncertainty of the calculations[54] was not discussed by the authors, so it is reasonable to use the experimental uncertainty[59] (20% or less).

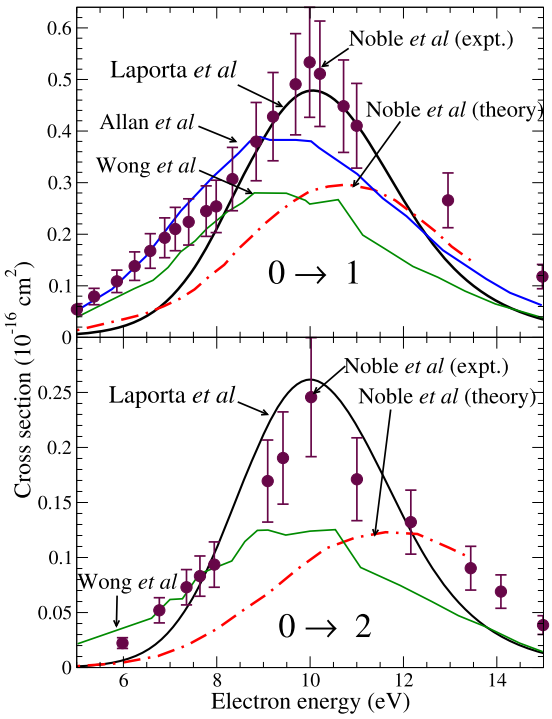

FIG. 6. Comparison of available data on vibrational excitation of O_2 starting from the ground vibrational level to $v = 1$ and 2. The figure shows data from three experimental studies by Noble *et al.*,[59] Wong, Boness, and Schulz ,[58] and Allan,[53] and from calculations by Noble *et al.*[59] and Laporta, Celiberto, and Tennyson.[54] The data from Ref. 54 are recommended, except the non-resonance part (1–8 eV and above 12 eV) of the 0–1 transition, where the experiment data by Noble *et al.*[59] are recommended.

Figure 6 compares the $v = 0 \rightarrow v' = 1$ and 2 cross sections[53] recommended in the previous review[10] with the cross section by Laporta, Celiberto, and Tennyson[54] (recommended in this review) and those of a few other studies. Figure 7 gives a few examples of the recommended cross sections in the lower-energy region of the $^2\Pi_g$ resonance. The complete data for the recommended cross sections are available in numerical form as supplementary material of the original study.[54]

2.6. Electronic excitation cross section

A particularity of molecular oxygen, compared to other atmospheric gases like N_2, NO, CO_2 or H_2O, is the presence of two low-lying metastable electronic states, $a^1\Delta_g$ and $b^1\Sigma_g^+$, with low excitation thresholds of 0.98 and 1.63 eV, respectively. Two O_2 bands lie on the red edge of the visible spectrum; these bands are used for remote sensing of Earth's atmosphere: the A-band centered at 762 nm, arising from the $b^1\Sigma_g^+(v = 0) \rightarrow X^3\Sigma_g^-(v = 0)$ transition,[65] and the B-band, 15 times weaker, centered around 690 nm and arising from the $b^1\Sigma_g^+(v = 1) \rightarrow X^3\Sigma_g^-(v = 0)$ transition.[66] As already mentioned, the IR part of the absorption spectrum, related to the excitation of the $a^1\Delta_g$ state, is used in the photodynamic treatment of melanoma.[5,6]

Higher in energy, as seen in forward-angle electron scattering spectra[67–69] (that are directly related to the photoabsorption), the so-called Herzberg's pseudo-continuum, resulting from excitation to the overlapping $c^1\Sigma_u^-$, $A'^3\Delta_u$ and $A^3\Sigma_u^+$ states, extends between

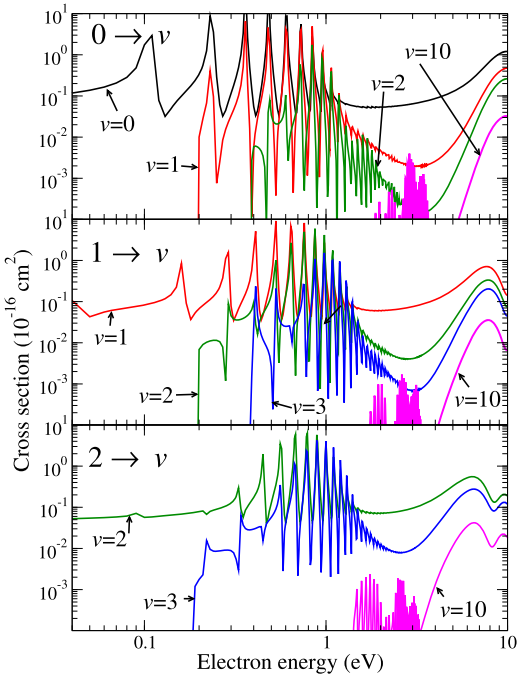

FIG. 7. Examples of recommended cross sections for vibrational excitation for several transition obtained by Laporta, Celiberto, and Tennyson.[54] The upper panel shows transitions from $v = 0$ to 0, 1, 2, and 10. The middle panel gives the transitions from $v = 1$ to 1, 2, 3, and 10, and the lower panel from $v = 2$ to 2, 3, and 10.

about 5 and 7 eV. Excitations to these states influence production of the O^- ion via dissociative electron attachment (DEA)[70] and the production of stratospheric ozone;[71] the de-excitation processes produce the equatorial night-glow.[72] Next, a much stronger structureless band in the forward-scattering electron spectra[68,73] extends from 7 to 9.5 eV and corresponds to the excitation to the $b^3\Sigma_u^-$ state (the Schumann–Runge continuum in optical spectra). Finally, still below the ionization threshold, two sharp peaks due to excitation to $E\,^3\Sigma_u^-$ in $v' = 0$ and $v' = 1$ vibrational states are visible in energy-loss electron spectra[68,73] at 10.0 and 10.3 eV, respectively. Detectable[74] in night-glows are also transitions between excited states, like $c^1\Sigma_u^- \rightarrow b^1\Sigma_g^+$.

In the reviews by Itikawa[10] and Brunger and Buckman,[12] as well as in a later review by Tanaka *et al.*,[46] recommended cross sections for electronic excitations were derived from experimental data. For excitation of the $a^1\Delta_g$ and $b^1\Sigma_g^+$ states from the ground state $X\,^3\Sigma_g^-$, the experimental data by Shyn and Sweeney[75] were recommended. The excitation energies of the $c^1\Sigma_u^-$, $A'\,^3\Delta_u$ and $A^3\Sigma_u^+$ states are close to each other (6.12, 6.27, and 6.47 eV, respectively[76]), so that it is difficult to separate contributions of individual states into measured results in energy-loss experiments. Thus, in the previous review, Itikawa[10] recommended only their sum. For excitation of the $^3\Sigma_u^-$ state and some higher electronic states, even though some experimental data are available,[75,77] Itikawa[10] did not recommend the data due to the large uncertainty. Therefore, the data recommended in the previous reviews[9,10,46] based on the experimental results are very limited, except for the $a^1\Delta_g$ and $b^1\Sigma_g^+$ states.

At present, first-principle calculations are an alternative to experiment in similar situations. There have been several theoretical studies on electronic excitation of O_2 by electron impact. Teillet-Billy, Malegat, and Gauyacq[76] used a multichannel effective range theory to model e-O_2 excitation. Machado *et al.*[78] employed the Schwinger variational iterative method and the distorted-wave approximation in their calculations. Furthermore, Noble and Burke,[56] Middleton *et al.*,[79] Tashiro, Morokuma, and Tennyson ,[80] Singh and Baluja,[81] Huang, Zhang, and Cheng[82] used versions of the UK molecular R-matrix code[64,83,84] to compute cross sections for excitation and de-excitation of O_2 electronic states for a large number of transitions.

All the cited theoretical calculations were preformed for a fixed internuclear distance, close to the equilibrium of O_2, situated near 2.287 a_0. A more accurate theoretical approach would have to account for the vibrational motion of the molecule. This will generally flatten the peaks seen in the fixed nuclei calculations. However, given that experimental results are scarce and, for higher excited states, have very large or unspecified uncertainties, the theoretical data can be recommended for electronic excitation of O_2.

In this review, we recommend theoretical cross sections obtained in the latest R-matrix study.[82] In the earlier study by Tashiro, Morokuma, and Tennyson,[80] very similar parameters as in the R-matrix approach were used. Hence the results of Refs. 80 and 82 are close to each other. In particular, optimized orbitals were employed in both studies, in contrast, for example, to another relatively recent study by Singh and Baluja,[81] in which Hartree–Fock orbitals were employed. The use of optimized orbitals produced more accurate excitation energies in Refs. 80 and 82. Consequently, we expect the excitation cross sections to also be more accurate.

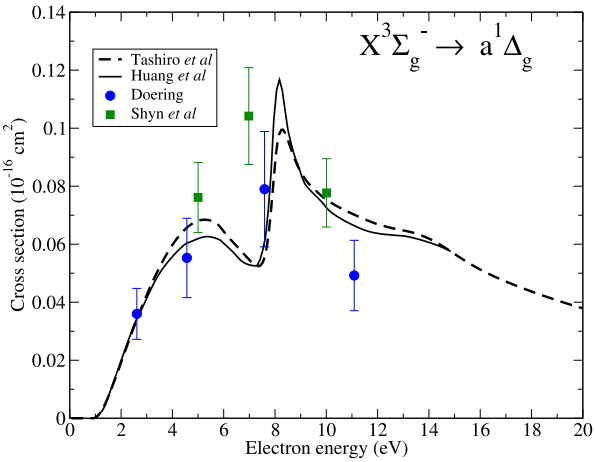

FIG. 8. Electronic excitation cross section for the $X^3\Sigma_g^- \rightarrow a^1\Delta_g$ transition. Solid line: Huang, Zhang, and Cheng[82] (recommended); dashed line: Tashiro, Morokuma, and Tennyson;[80] circles: experiment by Doering;[85] squares: experiment by Shyn and Sweeney.[75]

Figure 8 compares the recent theoretical results[80,82] and the available experimental data for the $X^3\Sigma_g^- \rightarrow a^1\Delta_g$ transition. The solid line represents the calculations by Huang, Zhang, and Cheng[82] (recommended), the dashed line the calculations by Tashiro, Morokuma, and Tennyson,[80] the circles the experiment by Doering,[85] and the squares the experiment by Shyn and Sweeney.[75] The previous review[10] recommended the latter experimental cross section.[75]

Figure 9 depicts the recent theoretical predictions[80,82] and the experimental[75] data for the $X^3\Sigma_g^- \rightarrow b^1\Sigma_g^-$ transition. For this transition, the previous review[10] also recommended the experimental cross sections.[75]

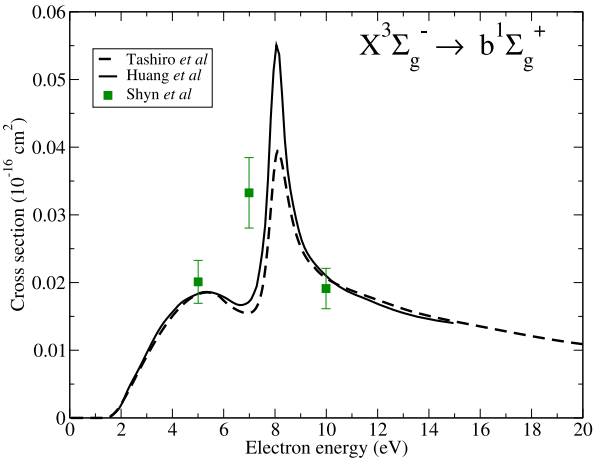

FIG. 9. Similar to Fig. 8 for the $X^3\Sigma_g^- \rightarrow b^1\Sigma_g^-$ transition. Solid line: Huang, Zhang, and Cheng[82] (recommended); dashed line: Tashiro, Morokuma, and Tennyson;[80] squares: Shyn and Sweeney.[75]

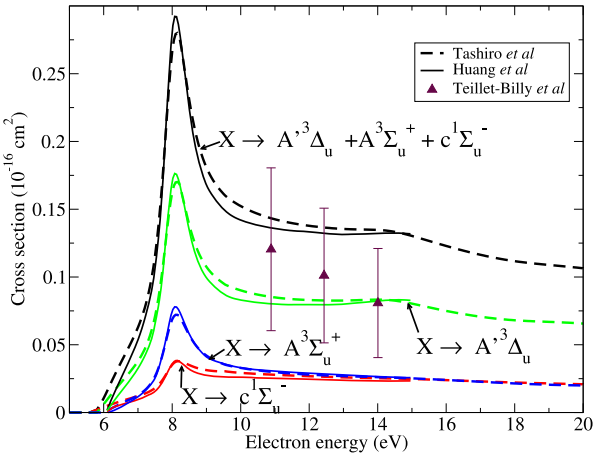

FIG. 10. Electronic excitation cross section for the $X^3\Sigma_g^- \rightarrow c^1\Sigma_u^-$ (red lines), $X^3\Sigma_g^- \rightarrow A^3\Sigma_u^+$ (blue lines), and $X^3\Sigma_g^- \rightarrow A'^3\Delta_u$ (green lines) transitions. Solid lines: Huang, Zhang, and Cheng[82] (recommended); dashed lines:Tashiro, Morokuma, and Tennyson.[80] Upper black curves are the sum of the three excitation cross sections while the triangles with uncertainties are measurements of this sum by Teillet-Billy *et al.*[86]

In Fig. 10, theoretical cross sections[80,82] for excitation of the $c^1\Sigma_u^-$, $A^3\Sigma_u^+$, and $A'^3\Delta_u$ states are shown. The black lines represent sums of the cross sections for the three transitions. The symbols in the figure are the experimental data,[86] which also represent the sum of the three contributions.

Figure 11 shows cross sections for transitions starting from the $a^1\Delta_g$ state, including the elastic process. In addition to the theoretical predictions, experimental data points[87] are shown for the $a^1\Delta_g \rightarrow b^1\Sigma_g^+$ and $a^1\Delta_g \rightarrow X^3\Sigma_g^-$ transitions. Figure 12 presents the

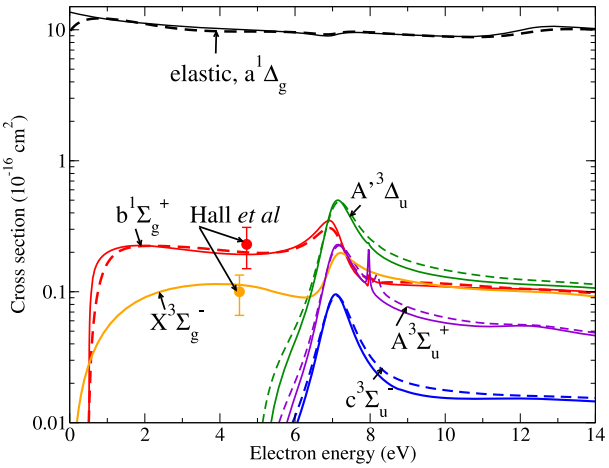

FIG. 11. Cross sections for elastic and inelastic transitions starting from the metastable $a^1\Delta_g$ state. Solid lines: Huang, Zhang, and Cheng[82] (recommended); dashed lines: Tashiro, Morokuma, and Tennyson.[80] Red and orange circles are the experimental data[87] for the $a^1\Delta_g \rightarrow b^1\Sigma_g^+$ and $a^1\Delta_g \rightarrow X\,^3\Sigma_g^-$ transitions, respectively.

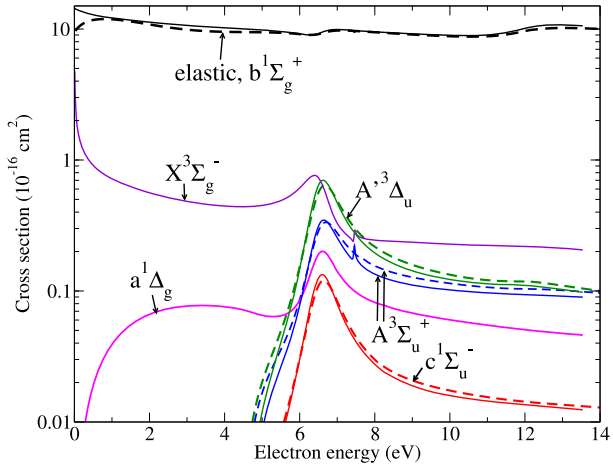

FIG. 12. Similar to Fig. 11 for the elastic and inelastic transitions starting from the metastable $b^1\Sigma_g^+$ state. The cross sections are taken from Ref. 80.

cross sections[80] for the elastic and inelastic transitions starting from the $b^1\Sigma_g^+$ state.

2.7. Neutral dissociation cross section

Photodissociation of the O_2 molecule in Earth's stratosphere is the key process for the formation of ozone. The oxygen molecule is characterized by a low dissociation energy (5.12 eV, see recent photodissociation studies[88]), as compared, for example, to N_2 (9.79 eV). O_2 is also an example of an interdependence of the electronic excitation and the dissociation of the molecule: all electric dipole allowed transitions lie above the first dissociation limit and appear to dissociate.[89]

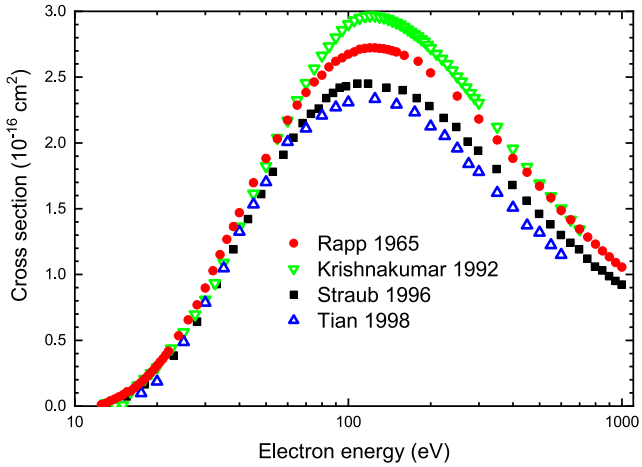

FIG. 14. TCS for electron impact ionization of the O_2 molecule. Solid (red) circles are the gross total (i.e., the overall current of ions) ionization cross section from Ref. 94; (green) open triangles are the counting (i.e., the sum of partial) ionization cross sections from Krishnakumar and Srivastava.[96] The (blue) open triangles are from Ref. 97. The (black) solid squares are the counting cross sections from Straub *et al.*[98] renormalized by Lindsay and Mangan.[17]

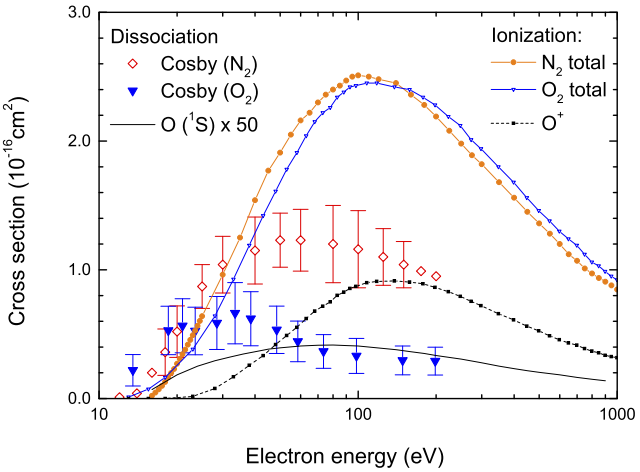

FIG. 13. Experimental TCS for dissociation of O_2 into neutral atoms. Absolute cross sections for the total dissociation for O_2 and N_2 are by Cosby,[89,90] while data for the production of the metastable O(^{1}S) atom are by LeClair and McConkey.[92] In comparison, the total ionization cross section in O_2 and N_2 is taken from the review by Lindsay and Mangan.[17]

Absolute cross sections for electron-impact dissociation into two neutral O atoms have been determined by Cosby.[89] He used a position-sensitive detector, allowing him to observe correlation between the dissociated fragments (but not allowing him to discriminate between their particular electronic state). Cosby[89] deduced that there are two (overall) dissociation channels: production of O(^{1}D) + O(^{3}P) fragments from electronically excited $b^3\Sigma_u^-$, $B'^3\Sigma_u^-$ and $2^3\Pi_u$ states of O_2, and production of O(^{3}P) + O(^{3}P) fragments from electronically excited $c^1\Sigma_u^-$, $A'^3\Delta_u$ and $A^3\Sigma_u^+$ states. The maximum cross section for total dissociation into neutrals amounts to 0.66×10^{-16} cm^2 at about 35 eV; the cross section for the production of the neutral fragment with a kinetic energy > 2.7 eV is ten times smaller at that energy.

Figure 13 compares the TCS for the dissociation into neutrals in O_2 by Cosby[89] with those in N_2 by the same author.[90] The total dissociation cross section for O_2 has a maximum of less than half of that for N_2, even though the ionization cross sections are almost identical for the two molecules. See our previous recommendations for N_2.[91]

Production of the metastable O(^{1}S) atom was measured by LeClair and McConkey.[92] As seen from Fig. 13, this cross section is a factor 50 smaller than the TCS for dissociation into neutrals determined by Cosby.[89] Recommended cross sections for the electron-impact dissociation of O_2 into neutral atoms are given in Table 6. The overall uncertainty of these values is ±35%.

2.8. Ionization cross section

Ionization of the oxygen molecule has been extensively studied, starting from early experiments by Tate and Smith.[93] The agreement between different datasets is generally quite good. Early measurements by Tate and Smith,[93] and by Rapp and Englander-Golden[94] yielded only a gross total (i.e., the total ion current produced).

TABLE 6. Recommended cross sections for the dissociation into neutrals of O_2. Data are from Cosby.[89] The uncertainty is about ±35%

Electron energy (eV)	Dissociation cross section (10^{-16} cm^2)	Electron energy (eV)	Dissociation cross section (10^{-16} cm^2)
13.5	0.220	48.5	0.534
18.5	0.529	58.5	0.444
21.0	0.565	73.5	0.366
23.5	0.525	98.5	0.331
28.5	0.587	148.5	0.296
33.5	0.663	198.5	0.291
38.5	0.610		

Later, mass selectors, like the sector magnetic field[95] or time-of-flight spectrometers,[96] also allowed partial cross sections, i.e., for single ions produced, to be determined. The disadvantage of the latter experiments was that they required normalization procedures, usually to helium[96] or argon.[95] The most recent generation of experiments[97–101] uses position-sensitive detectors, which allow the simultaneous tracking of all the ions produced.

Figure 14 compares total ionization cross sections from different laboratories. Note that measurements by Rapp and Englander-Golden[94] are gross total ionization cross sections (i.e., the total current of ions), while those by Krishnakumar and Srivastava,[96] Tian and Vidal,[97] and Straub *et al.*[98] are the sum of all partial cross sections. Correcting the gross total of Rapp and Englander-Golden[94] for double ionization[97] makes their results almost coincide with the counting cross sections of Straub *et al.*[98] However, an uncertainty of about 5% in the total (counting) ionization cross section[98] still remains.

Ionization into the parent ion, i.e., O_2^+, dominates the total ionization cross section; see Fig. 15. The two recent measurements[97,98] almost coincide; the discrepancy with other earlier sets[95,96] can be

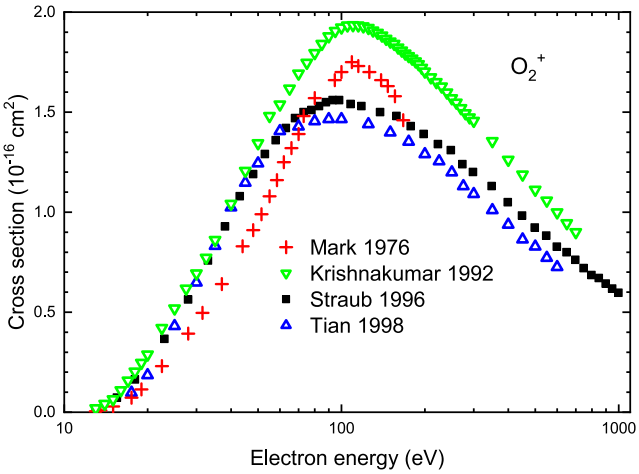

FIG. 15. Partial cross section for the formation of the O_2^+ ion. Red crosses represent Ref. 95, for the other symbols see Fig. 14.

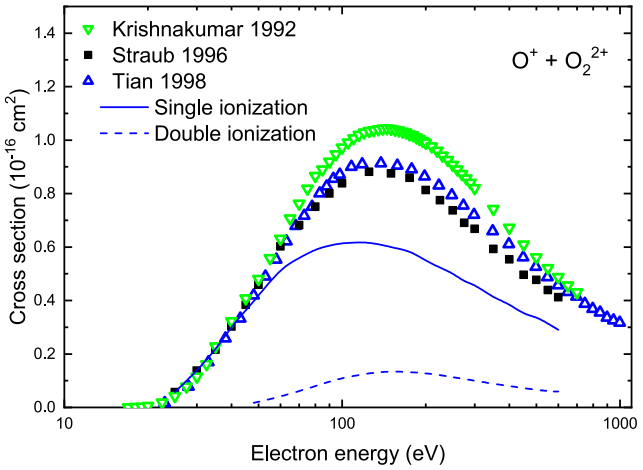

FIG. 16. Partial cross section for the formation of the O^+ ion. The signal from O^+ ions is experimentally indistinguishable from the O_2^{2+} signal. For the symbols, see Fig. 14. The lines represent the production of O^+ ions via single, i.e., $O^+ + O$, or double ($O^+ + O^+$) ionization, by Tian and Vidal.[97]

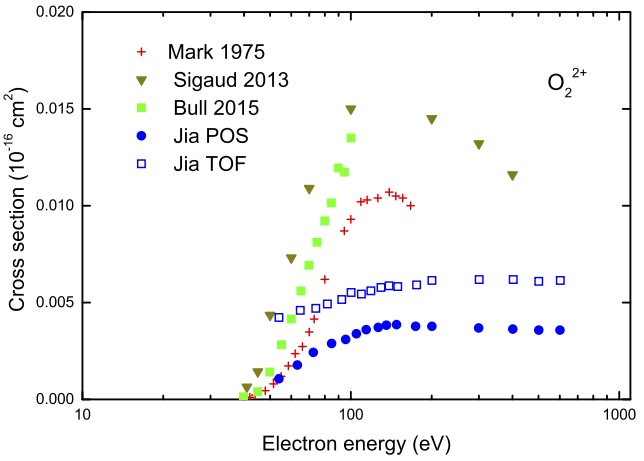

FIG. 17. Partial cross section for the formation of the O_2^{2+} ion. Red crosses;[95] inverted dark yellow triangles;[100] green squares;[99] open and closed blue circles[101] by time-of-flight and position-sensitive methods, respectively. The data were read from the figures in the papers.

attributed to the normalization procedures mentioned above and/or differences in the detection efficiency of the mass spectrometers used.

Doering and Yang[102] measured the energy of secondary electrons and thereby determined the electronic state of the O_2^+ ion. At 100 eV, the branching ratios between the ground ionic X $^2\Pi_u$ and excited $a^4\Pi_u$ and $b^4\Sigma_g^-$ states (with respective ionization thresholds[103,104] 12.2, 16.3, and 18.4 eV) are 9:5:2.

The production of O^+ ions (in the majority of experiments indistinguishable from the O_2^{2+} ion) is roughly half of the O_2^+ yield, see Fig. 16. The same figure shows the contribution to the production of the O^+ ion via single, i.e., $O^+ + O$, or double ($O^+ + O^+$) ionization.[97]

The early measurement on $^{17}O^{16}O$ by Märk[95] and the recent experiments with position-sensitive detectors[99–101] allowed the separate yield of O_2^{2+} ions to be measured: at 100 eV it amounts to roughly 10% of the O^+ signal.[99] However, the spread between different data obtained with different methodologies is large; see Fig. 17. Hence, we are unable to recommend data for this case.

The O_2^{2+} ion has a bond energy[105] of −2.65 eV. Therefore, it is metastable with a lifetime[99] of about 1–2 μs. Techniques using angular coincidence[106,107] and measurements of the kinetic energy release[99] allows the identification of the decay pathways of molecular ions. According to Bull, Lee, and Vallance,[99] O^+ ions are (at 100 eV) predominantly produced via dissociation of the $B^2\Sigma_g^-$ excited state of the O_2^+ ion, with dissociation asymptotes $O^+(^4S) + O(^3P)$ and $O^+(^4S) + O(^1D)$. The precursors of the most intense asymptotic channel $O^+(^2D) + O(^3P)$ is unclear. In total, at 100 eV, 68% of atomic ions are produced in the ground ^4S state, 25% in the ^2D state, and 8% in the ^2P electronically excited states.

Figure 18 shows the partial cross section for the formation of the doubly charged atomic ion O^{2+}. Its maximum yield is roughly 1% of the O_2^+ signal. Recent measurements (not shown in the figures) by Lomsadze *et al.*[108] coincide with those by Straub *et al.*[98] Studies of O_2 molecules heated in a shock wave,[109] up to 5000 K, did not reveal, within the experimental uncertainty, any difference in ionization, as compared to 300 K.

Our recommended ionization cross sections are based on the review by Lindsay and Mangan[17] and shown in Fig. 19. The values are given in Table 7. The uncertainty is 5% on the total ionization and the O_2^+ yield, and 7% on the O^+ and 10% on the O^{2+} yield.

2.9. Dissociative electron attachment cross section

In 1965, Rapp and Briglia[110] derived the DEA cross sections of O_2 using the method of total ionization measurement. The cross sections show a single peak centered at the electron energy of 6.5 eV with a cross section of 1.41×10^{-18} cm^2. Rapp and Briglia did not

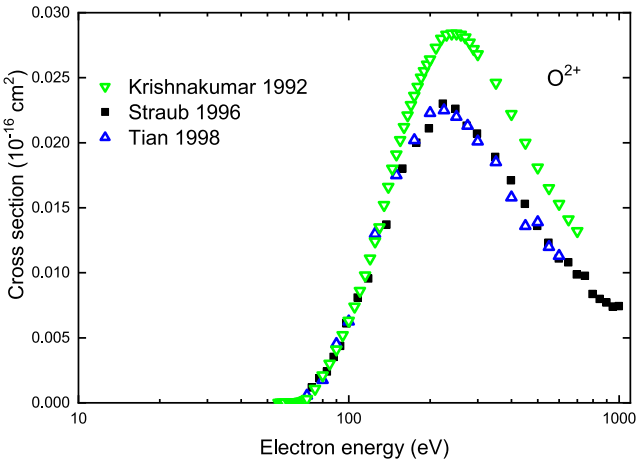

FIG. 18. Partial cross section for the formation of the O^{2+} ion. For symbols, see Fig. 14.

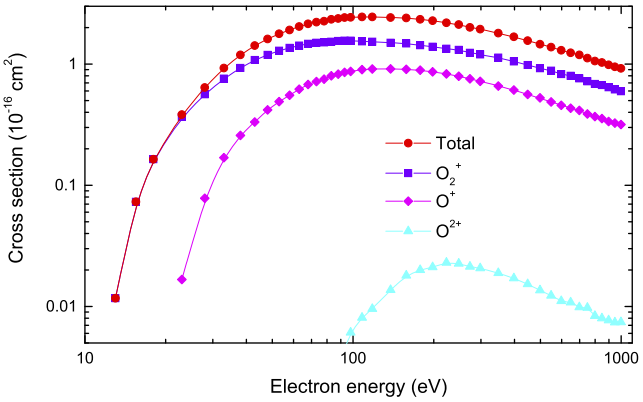

FIG. 19. Recommended total and partial cross sections for ionization of the O_2 molecule. Data from the review by Lindsay and Mangan.[17] Recommended values are given in Table 7.

provide an uncertainty for this measurement. We conservatively suggest that it would be no more than 20%, inferred from their experiments using the positive-ion measurement device that was also used in deriving the DEA cross section. In the same year, Christophorou *et al.*[111] measured the DEA cross sections of O_2 using a swarm setup; these cross sections are in agreement with the results of Rapp and Briglia. The DEA of ground state O_2 occurs via the following process: $e^- + O_2(X^3\Sigma_g^-) \rightarrow O_2^{-*} \rightarrow O^-(^2P) + O(^3P)$.

Laporta, Celiberto, and Tennyson[112] calculated vibrational excitation and DEA cross sections as function of the initial O_2 vibrational state using resonance curves computed by the R-matrix method. For low vibrational states, they found that DEA largely goes via the $^4\Sigma_u^-$ resonance state but for vibrationally excited states DEA can occur with a much lower threshold via the low-lying $^2\Pi_u$ resonance state of O_2^-.

To determine the angular distribution of O^- from DEA to O_2, Van Brunt and Kieffer[113] assumed the $^2\Pi_u$ symmetry to provide the dominant contribution. Later, Prabhudesai, Nandi, and Krishnakumar[114] obtained evidence for the involvement of the $^4\Sigma_u^-$ resonance in DEA of O_2 for the first time from angular distribution measurements of O^- ions over the entire 2π angular range by employing the velocity map imaging technique. Some DEA experiments with hot O_2 or with metastable oxygen molecules[115,116] were reported, but they are not included in the present evaluation. Since Rapp and Briglia[110] with Christophorou *et al.*[111] provide the only absolute DEA cross sections, the previous reviews[10,117] recommended the DEA cross sections of O_2 by Rapp and Briglia.[110] We recommend the same cross sections, which are given in Fig. 20 and Table 8.

3. Atomic Oxygen

Miller and Banks[118] note that "atomic oxygen is the predominant species in low-Earth orbit and is contained in the upper atmosphere of many other planetary bodies." Together with its ion, it is also the dominant species in Earth's ionosphere. In the ionosphere of Venus, a small proportion of oxygen atoms (≈1%) assures production of O_2^+ ions via the reaction with CO_2^+ ions[119] as

TABLE 7. Recommended cross sections in (10^{-16} cm^2) for ionization of O_2. The data are from Ref. 17. The uncertainty is 5% on the total ionization and the O_2^+ partial cross section, 7% on the O^+, and 10% on the O^{2+} cross section. We are unable to recommend values for O_2^{2+} ions due to a large spread in recent data; see Fig. 17

Energy (eV)	O_2^+	O^+ ($+O_2^{2+}$)	O^{2+}	Total
13.0	0.0117			0.0117
15.5	0.0730			0.0730
18.0	0.164			0.164
23	0.366	0.0167		0.383
28	0.563	0.0781		0.641
33	0.758	0.169		0.927
38	0.929	0.258		1.19
43	1.08	0.333		1.42
48	1.19	0.419		1.61
53	1.29	0.490		1.78
58	1.36	0.553		1.91
63	1.42	0.621		2.04
68	1.47	0.679		2.15
73	1.50	0.717	0.001 18	2.22
78	1.51	0.751	0.001 89	2.26
83	1.53	0.801	0.002 41	2.34
88	1.55	0.827	0.003 52	2.38
93	1.56	0.855	0.004 38	2.42
98	1.56	0.871	0.006 10	2.43
108	1.54	0.900	0.008 08	2.45
118	1.53	0.910	0.009 56	2.45
138	1.50	0.913	0.013 7	2.42
158	1.48	0.905	0.018 0	2.40
178	1.43	0.891	0.020 0	2.34
198	1.39	0.864	0.021 1	2.28
223	1.34	0.830	0.0230	2.19
248	1.31	0.794	0.022 6	2.12
273	1.24	0.755	0.021 3	2.01
298	1.20	0.721	0.020 7	1.94
348	1.13	0.659	0.018 9	1.80
398	1.05	0.611	0.017 1	1.68
448	0.983	0.562	0.015 3	1.56
498	0.923	0.526	0.013 6	1.46
548	0.882	0.487	0.012 3	1.38
598	0.827	0.457	0.011 1	1.30
648	0.800	0.432	0.010 8	1.24
698	0.761	0.415	0.009 87	1.19
748	0.720	0.388	0.009 77	1.12
798	0.686	0.369	0.008 37	1.06
848	0.671	0.355	0.007 99	1.03
898	0.643	0.336	0.007 70	0.987
948	0.617	0.326	0.007 40	0.950
998	0.597	0.317	0.007 43	0.922

$$CO_2^+ + O \rightarrow O_2^+ + CO. \quad (2)$$

In the Earth's troposphere, the metastable ^1D state triggers production of OH radicals, which are the main oxygenating agent via the reaction[120]

$$O(^1D) + H_2O \rightarrow 2\ OH. \quad (3)$$

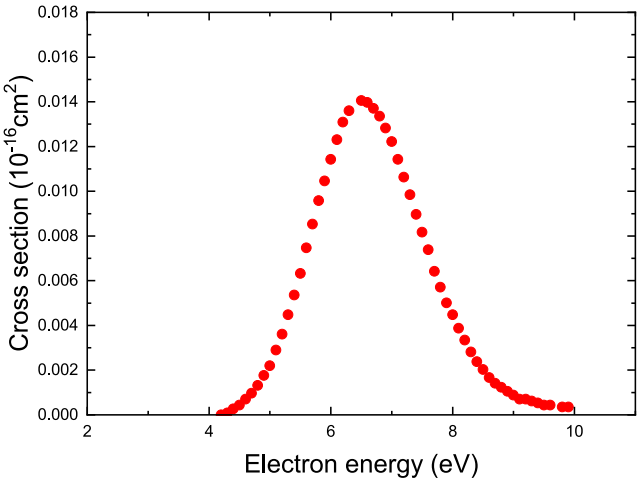

FIG. 20. Recommended DEA cross sections for O_2.

An interplay of the 557.7 nm (green) and 630.0 nm (red) emission lines of atomic oxygen may explain the variation of colors in the boreal aurora, while quiet-time airglow continuum may be due to the chemiluminescence from the reaction[121]

$$O + NO \rightarrow NO_2. \quad (4)$$

Measurements of total, state-specific angle-integrated, and angle-resolved DCS for atomic oxygen are subject to much higher uncertainty than those for molecular oxygen. Therefore, few experimental results are available. Sunshine, Aubrey, and Bederson[28] used a recoil-beam method to measure TCS, with a stated uncertainty of ±20%. Williams and Allen[122] employed an electrostatic monochromator and an orientable detector to determine both elastic and TCS. Even if the uncertainty of such a method is usually 20%, their[122] TCS at low energies for molecular oxygen agree pretty well with our recommended values, see Fig. 1. However, as the atmospheric processes depend primarily on the specific electronic state of the oxygen atom, and such data are unavailable experimentally, we base our discussion in this chapter on comparison of theoretical results.

3.1. Total cross section

Figure 21 shows the TCS, as well as the contributing parts originating from elastic, elastic plus excitation, and ionization processes. The situation depicted here is quite typical. Only a few experimental data, often with substantial error bars, are generally available, and they may be insufficient to be used in a comprehensive collisional-radiative model (CRM). Not surprisingly, the situation deteriorates even more when it comes to state- and angle-resolved data, as will be shown further below.

Many theoretical approaches, on the other hand, are limited to particular energy ranges. The standard close-coupling method, with only a few discrete physical target states in the expansion, is generally suitable at low energies below the ionization threshold, while perturbative Born-based approaches are more appropriate for higher energies, particularly for optically allowed transitions.

TABLE 8. Recommended DEA cross sections for O_2. The uncertainty is no more than 20%

Electron energy (eV)	DEA (10^{-16} cm^2)	Electron energy (eV)	DEA (10^{-16} cm^2)
4.2	0.00×10^{-00}	7.1	1.14×10^{-2}
4.3	8.79×10^{-5}	7.2	1.06×10^{-2}
4.4	2.64×10^{-4}	7.3	9.84×10^{-3}
4.5	4.39×10^{-4}	7.4	8.96×10^{-3}
4.6	7.03×10^{-4}	7.5	8.17×10^{-3}
4.7	9.67×10^{-4}	7.6	7.38×10^{-3}
4.8	1.32×10^{-3}	7.7	6.41×10^{-3}
4.9	1.76×10^{-3}	7.8	5.71×10^{-3}
5.0	2.20×10^{-3}	7.9	5.01×10^{-3}
5.1	2.90×10^{-3}	8.0	4.48×10^{-3}
5.2	3.60×10^{-3}	8.1	3.87×10^{-3}
5.3	4.48×10^{-3}	8.2	3.34×10^{-3}
5.4	5.36×10^{-3}	8.3	2.81×10^{-3}
5.5	6.33×10^{-3}	8.4	2.37×10^{-3}
5.6	7.47×10^{-3}	8.5	2.02×10^{-3}
5.7	8.52×10^{-3}	8.6	1.67×10^{-3}
5.8	9.58×10^{-3}	8.7	1.41×10^{-3}
5.9	1.05×10^{-2}	8.8	1.23×10^{-3}
6.0	1.14×10^{-2}	8.9	1.05×10^{-3}
6.1	1.23×10^{-2}	9.0	8.79×10^{-4}
6.2	1.31×10^{-2}	9.1	7.03×10^{-4}
6.3	1.36×10^{-2}	9.2	7.03×10^{-4}
6.5	1.41×10^{-2}	9.3	6.15×10^{-4}
6.6	1.40×10^{-2}	9.4	5.27×10^{-4}
6.7	1.37×10^{-2}	9.5	4.39×10^{-4}
6.8	1.34×10^{-2}	9.6	4.39×10^{-4}
6.9	1.28×10^{-2}	9.8	3.51×10^{-4}
7.0	1.22×10^{-2}	9.9	3.51×10^{-4}

As will be discussed and illustrated further in the subsections below, we believe that the B-spline R-matrix with pseudo-states model of Tayal and Zatsarinny[123] produced by far the most comprehensive and reliable dataset. In this model, 19 spectroscopic bound states were coupled with 1097 pseudo-states representing the target continuum and core-excited autoionizing states up to about 50 eV above the ionization threshold. This model will be referred to as BSR-1116 below.

3.2. Elastic scattering and momentum transfer cross sections

We start this section with angle-differential elastic cross sections (DCSs), since those were measured for five energies in the experiment carried out by Williams and Allen.[122]

Figure 22 shows a comparison of their data with predictions from the very elaborate B-spline R-matrix (BSR) calculation performed by Tayal and Zatsarinny[123] mentioned above. That calculation is an update on previous work by the same authors[125] and another one by Plummer *et al.*[126] Based on the structure description (energy levels and oscillator strengths) given in the tables

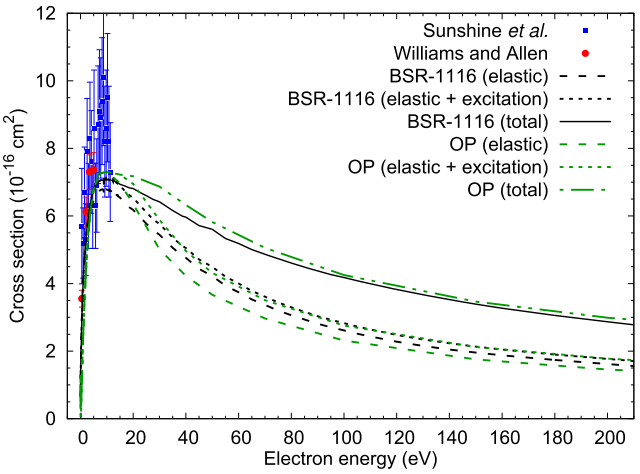

FIG. 21. Angle-integrated total (elastic + excitation + ionization) cross sections for electron collisions with oxygen atoms in the $(2p^4)\ ^3P$ ground state. The experimental data are from Sunshine *et al.*[28] and Williams and Allen.[122] The theoretical predictions are from Tayal and Zatsarinny[123] (BSR-1116) and Blanco and García[124] using a complex optical model potential (OP).

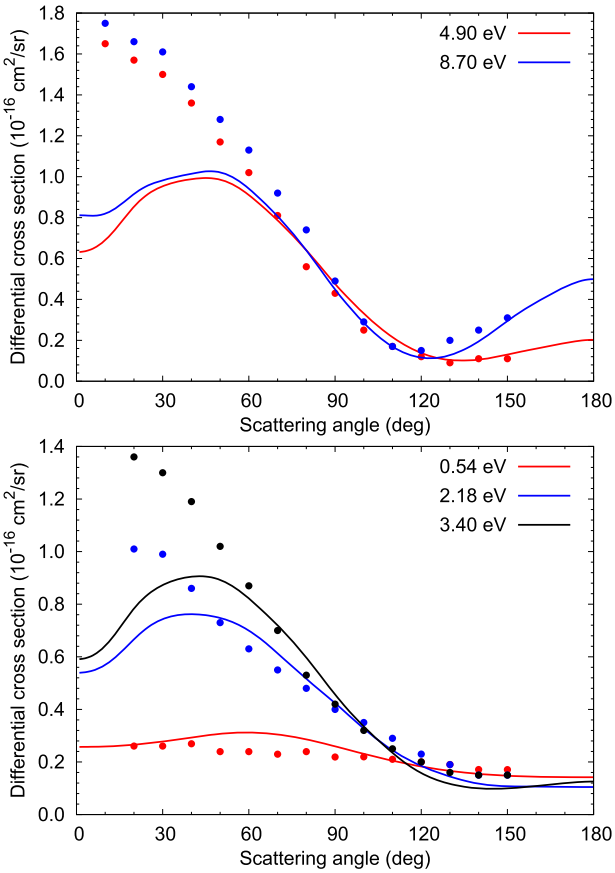

FIG. 22. Angle-differential elastic cross sections for electron collisions with atomic oxygen in the $(2p^4)^3P$ ground state for the five energies measured by Williams and Allen[122] (dots). The experimental data are compared with the theoretical predictions from Tayal and Zatsarinny[123] (solid lines).

by Tayal and Zatsarinny,[123] we put a high level of confidence in their work. Since relativistic effects are almost certainly negligible at the level of accuracy desired for the collisions of interest in the present assessment, it seems unlikely that any further improvement of the theoretical model would lead to significant changes in the predictions.

Looking at Fig. 22, which we generated from the transition-matrix elements available to us, we see overall good agreement between experiment and theory for scattering angles larger than about 60°, while there are significant discrepancies at smaller angles. In particular, theory predicts that the DCS decreases toward small scattering angles, while the experimental data keep increasing, with a likely maximum at or near the forward direction. We checked that this is not an issue of an insufficient number of partial waves included in the calculation.

We note that Plummer *et al.*[126] made similar predictions in their presumably best calculation [Fig. 3(e) of their paper]. Consequently, we favor theory over experiment in this case. In fact, Fig. 23 shows a contour plot of the DCS on a narrow energy-angle grid. Only at the high end of this energy scale does the DCS approach its maximum near the forward direction. The numerical data used to generate this figure for 31 energies up to 20 eV are available in the supplementary material.

The angle-integrated elastic (ICS) and MTCS are presented in Fig. 24. The larger experimental DCS for angles below 60° are consistent with the generally larger values reported by Williams and Allen[122] compared to theory. This is particular visible in the ICS, while the factor $1 - \cos\theta$ in the angle-differential form of the MTCS reduces the effect in the MTCS. The BSR predictions are available on a narrow energy grid up to 200 eV.

3.3. Selected excitation cross sections

We now select a few excitation cross sections to illustrate the general situation. The figures are based on those of Tayal and Zatsarinny,[123] where more can be found. The datafile in the supplementary material contains results for many more state-to-state transitions that would likely be needed to set up a complete CRM. In fact, for such a model, emission cross sections, i.e., accounting for the population of excited states via cascading, may be more suitable than the direct excitation cross sections the present manuscript is devoted to. Some emission cross sections were shown by Tayal and Zatsarinny,[123] more can be found in the supplementary material, and many more can be generated from the energy levels and oscillator strengths given therein.

Figure 25 shows two examples of excitation cross sections for optically allowed transitions from the $(2p^4)\ ^3P$ ground state. While the few available experimental data agree well with each other, we note the large error bars (up to ≈30%). Noteworthy, increasing the number of coupled states drastically reduces the theoretical predictions, in particular for the $(2p^4)\ ^3P \rightarrow (2p^3 3s)\ ^3D^o$ transition. Even though the results from the most extensive BSR calculation with 1116 coupled states lie significantly below the four points (two from each experiment, with the measured value for 30 eV barely agreeing

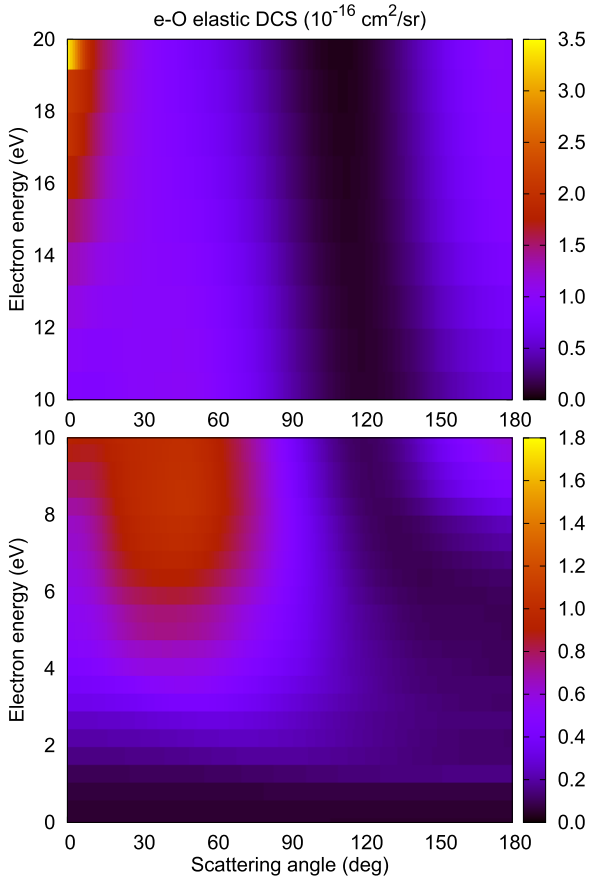

FIG. 23. Contour maps of the angle-differential elastic cross section for electron collisions with atomic oxygen in the $(2p^4)^3P$ ground state. The data were generated from the transition-matrix elements of Tayal and Zatsarinny.[123] Note the different color scales in the energy ranges 10–20 eV (top) and 0–10 eV (bottom) that were used to clearly illustrate the behavior of the DCS at small angles.

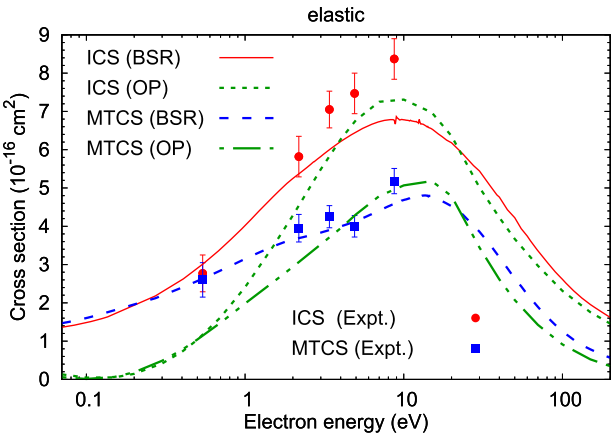

FIG. 24. Angle-integrated elastic and MTCS for electron collisions with atomic oxygen in the $(2p^4)^3P$ ground state. The experimental data of Williams and Allan[122] are compared with the recommended theoretical BSR predictions from Tayal and Zatsarinny[123] and the optical-potential (OP) calculation of Blanco and Garcia.[124] See text for details.

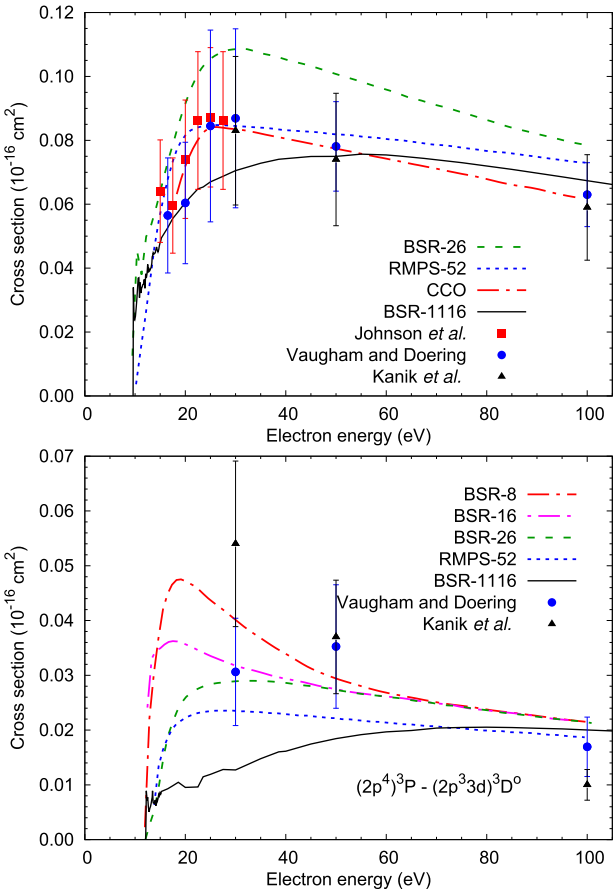

FIG. 25. Angle-integrated excitation cross sections for the optically allowed $(2p^4)\ ^3P \rightarrow (2p^3 3s)\ ^3S^o$ (top) and $(2p^4)\ ^3P \rightarrow (2p^3 3s)\ ^3D^o$ (bottom) transitions. The numbers behind the models indicate the number of states in the close-coupling expansion. The experimental data are from Johnson *et al.*,[127] Vaugham and Doering,[128] and Kanik *et al.*,[129] while the theoretical predictions are: BSR-8, BSR-16, and BSR-26;[125] RMPS-52;[130] CCO;[131] BSR-1116.[123]

with each other within the error bars given), we recommend those theoretical predictions.

Figure 26 shows three examples of excitation cross sections for optically forbidden transitions from the $(2p^4)\ ^3P$ ground state. The situation regarding the experimental data is similar to the previous examples. There are only a few data points that often, though not always, agree with each other within the large error bars given. Except for the $(2p^4)\ ^3P \rightarrow (2p^3 3s)\ ^5S^o$ transition, the convergence of the theoretical predictions with the number of coupled states is quite good, with the largest calculation generally predicting the smallest cross section for individual discrete state-to-state transitions, in particular from the ground state. This is a well-known result, which makes sense in light of the fact that the TCS (see above) tends to be rather stable with regard to variations in theoretical models. Consequently, the flux that can go into additional channels needs to be made up for. Once again, we recommend the BSR-1116 results, which are available for many energies in the supplementary material, for modeling applications.

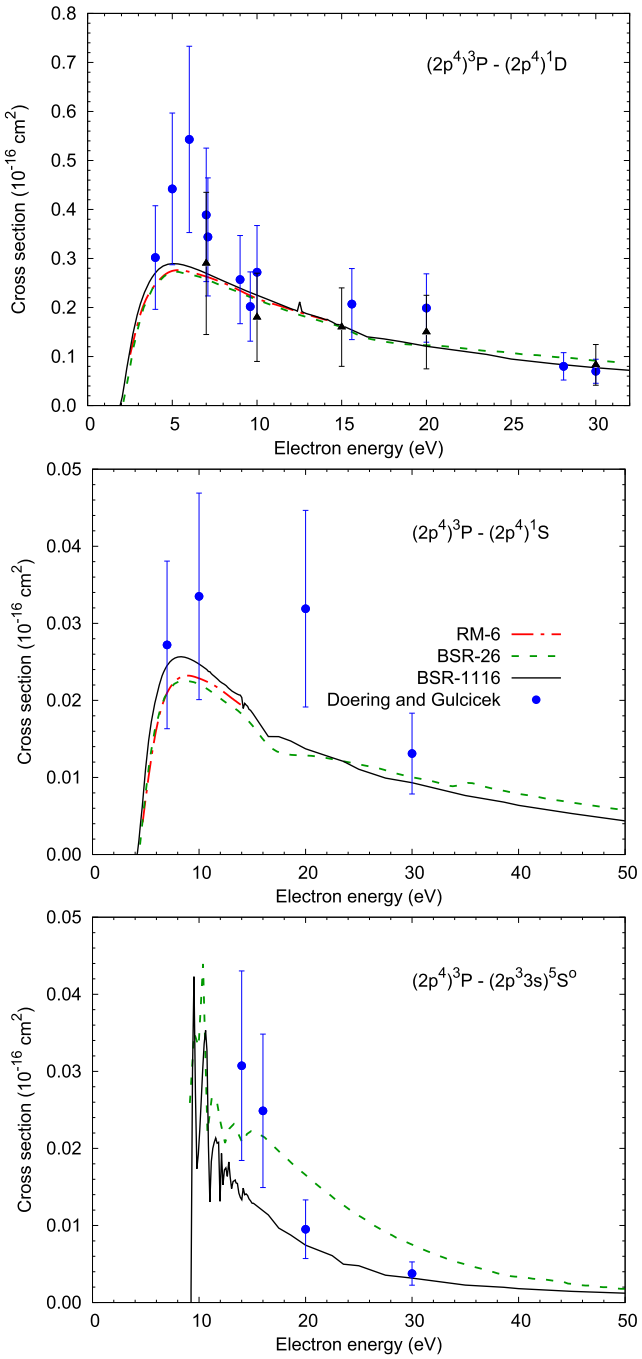

FIG. 26. Angle-integrated excitation cross sections for the optically forbidden $(2p^4)\ ^3P \rightarrow (2p^4)\ ^1D$ (top), $(2p^4)\ ^3P \rightarrow (2p^4)\ ^1S$ (center), and $(2p^4)\ ^3P \rightarrow (2p^3 3s)\ ^5S^o$ (bottom) transitions. The experimental data are from Doering,[132] Shyn and Sharp,[133] and Doering and Gulcicek[134,135] for the ^1S and $^5S^o$ final states, respectively. The theoretical predictions are: RM-6,[126] BSR-26,[125] and BSR-1116.[123]

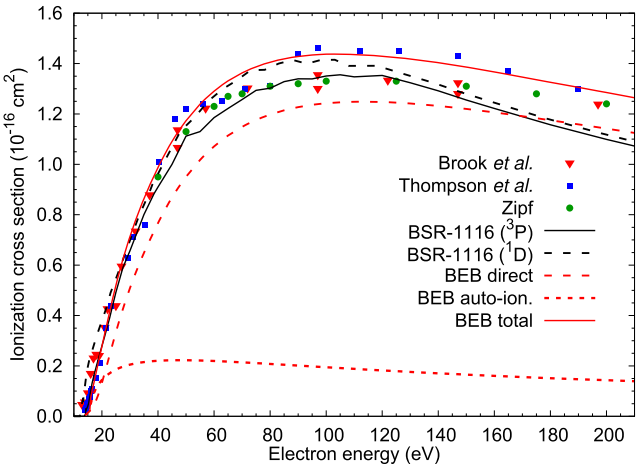

FIG. 27. Angle-integrated ionization cross section for electron collisions with oxygen atoms in the $(2p^4)\ ^3P$ ground state. The experimental data are from Refs. 136, 138, and 139 and the BEB results from Kim and Desclaux.[137] Also shown are the BSR-1116 predictions from Tayal and Zatsarinny[123] for both the $(2p^4)^3P$ and $(2p^4)^1D$ initial states.

3.4. Ionization cross sections

We finish this section with the ionization cross section for electron collisions with oxygen atoms in the $(2p^4)\ ^3P$ ground state. As is often the case (see Fig. 21 above), the ionization cross section is generally larger than even the sum of all individual excitation cross sections, and experimental data from different studies tend to agree reasonably well with each other. Here, too, the BSR-1116 predictions appear to be preferable, with the additional benefit of

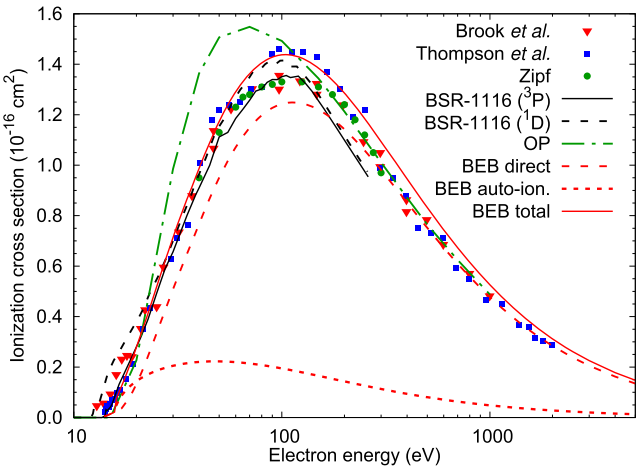

FIG. 28. Same as Fig. 27 on an extended logarithmic energy scale. Also shown are the optical-potential (OP) calculations from Blanco and García.[124]

them being available on a dense and extensive energy grid. While we do not show such results here, we note that the TCS includes de-excitation processes as well. For details, see the paper by Tayal and Zatsarinny.[123]

Experimental and theoretical ionization cross sections for atomic oxygen are compared in Figs. 27 and 28 on linear and logarithmic energy scales, respectively. The overall agreement is good. Brook *et al.*[136] observed an ion signal already at 12.9 eV, i.e., below the ionization threshold (13.62 eV) of the $(3p^4)^3P$ ground state. They also mention the possibility of ionization from the metastable $(3p^4)^1D$ state. For this reason, we also include the BSR-1116[123] cross section for ionization of this state. The Bethe–Born binary encounter model (BEB) of Kim and Desclaux[137] agrees well with the experimental total cross ionization cross section, provided the contribution of ionization plus electronic excitation is added. The formation of the O^{2+} ions in the energy range 200–2000 eV amounts to about 3% of that of the O^+ ions.[136,138]

4. Summary and Future Work

As shown in this review, electron interactions with oxygen (both molecular and atomic) show several unusual features compared to other species.

For the molecule, the most prominent features in the energy range below 1 eV (i.e., in the "infra-red" range) are sharp resonant structures that are visible in the total and vibrational cross sections, due to a temporary capture of the interacting electron by the O_2 target. Sharp resonant enhancements (at energies above 6 eV) are also present in electronic excitation cross sections, both for optically allowed and forbidden transitions. Low values of the energy thresholds for the two long-lived singlet excited states and the small value for the dissociation into neutral atoms require, for any modeling of oxygen plasma or Earth's atmosphere, also the inclusion of cross sections for excited states, oxygen atoms and ions. We note that cross sections for the transition from the electronically excited states are particularly high (and show the transitions have low excitation thresholds). However, for successful modeling, more precise lifetime values of these species should be derived from spectroscopic data.[66] Due to the importance of the oxygen molecule, there has been a significant amount of work performed on nearly all cross sections. Therefore, we are able to make recommendations as summarized in Fig. 29. The one exception concerns the weak electron impact rotational excitation process, for which only estimates based on a very simplified theoretical treatment are available.

Figure 30 shows a selection of the most important recommended cross sections for the oxygen atom. For the elastic, momentum-transfer, and all excitation cross sections, we recommend the BSR-1116 predictions. They are from a highly sophisticated theoretical model, with an accurate target structure description, and have been checked for convergence regarding the number of states in the close-coupling expansion. The results are available on a narrow energy grid between the respective thresholds and 200 eV, beyond which they can be extended, if necessary, using the known dependence of such cross sections at high energies. Alternatively, the high-energy (200 eV and above) predictions of the optical-potential (OP) model by Blanco and García[124] could be used. There is a small discontinuity to be seen in the graph, which is due to the BSR-1116 and OP results not matching up perfectly at 200 eV. For ionization,

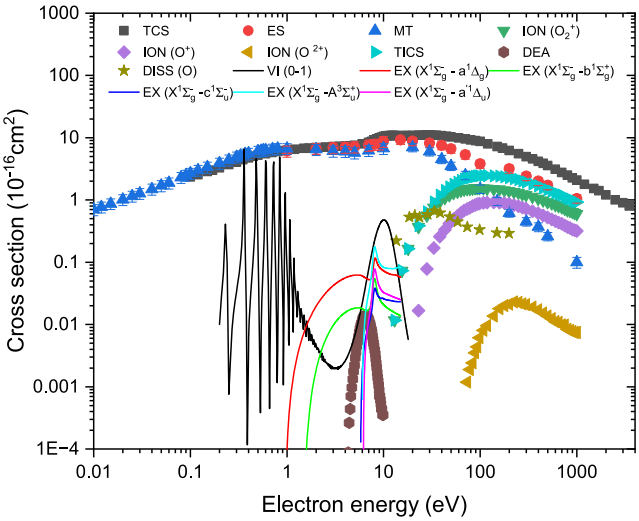

FIG. 29. Recommended angle-integrated cross sections for the oxygen molecule.

we recommend the most recent experimental data of Thompson *et al.*,[138] which agree very well with the BEB predictions of Kim and Desclaux.[137] Overall, we expect the recommended cross sections to be accurate to at least 20% for those that are sufficiently large to seriously matter in CRM models.

We specifically mention again the surprisingly high electron-impact ionization cross section for the oxygen atom, which is about twice as large as that for the O_2 molecule. This may explain why the O^+ ion accounts for almost all ionic species in Earth's atmosphere at an altitude of 500 km altitude. However, possible reactions with other atmospheric components certainly depend on the specific electronic state of the oxygen atoms. More research is needed before definite conclusions can be drawn.

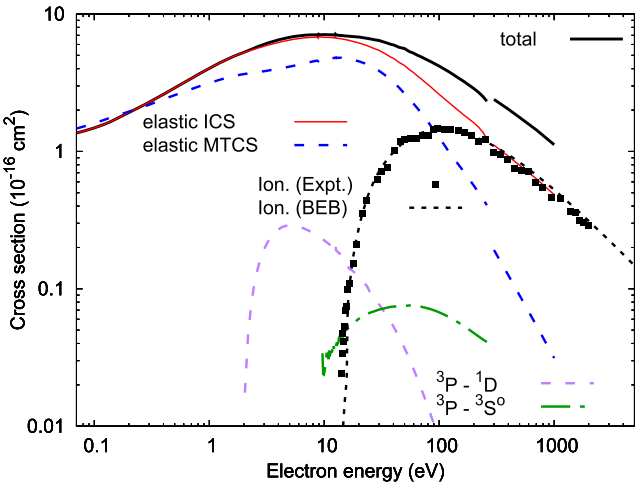

FIG. 30. Selected examples of recommended angle-integrated cross sections for the oxygen atom. See text for details.

Recent flybies[140] near Ganimede showed that interactions of energetic electrons with oxygen species may dominate atmospheric processes also on Jupiter's moons. Hence, data on electron scattering from oxygen may prove to be needed even more in astrophysics than in geophysics.

5. Supplementary Material

See supplementary material for recommended electron-impact collision cross section datasets for O and O_2 across various collisional processes.

Acknowledgments

This research was partially supported by the Plasma Fundamental Technology Research Project through the Korea Institute of Fusion Energy (KFE) funded by the Ministry of Science and Technology Information and Communication, Republic of Korea (2710094992). It was also partially funded by the U.S. National Science Foundation under Grants Nos. PHY-2110279 (V.K.), PHY-2102188 (V.K.), PHY-2110023 (K.B.), and PHY-2408484 (K.B.). G.P.K. thanks Eng. Klaudia Gackowska for retrieving numerical data and Professor Piotr Żuchowski from the Excellence Center for Astrochemistry of NCU for financial support.

Finally, the complete validation of the present cross sections, both for the molecule and the atom, may be done via their implementations in modeling laboratory plasma[47] and atmospheric[20] processes.

6. Author Declarations

6.1. Conflict of Interest

The authors have no conflicts to disclose.

7. Data Availability

The data that support the findings of this study are available from the corresponding author upon reasonable request and its supplementary material.

8. References

[1] M. Meftah, L. Dam'e, D. Bolsée, A. Hauchecorne, N. Pereira, D. Sluse, G. Cessateur, A. Irbah, J. Bureau, M. Weber, K. Bramstedt, T. Hilbig, R. Thiéblemont, M. Marchand, F. Lefèvre, A. Sarkissian, and S. Bekki, "SOLAR-ISS: A new reference spectrum based on SOLAR/SOLSPEC observations," Astron. Astrophys. **611**, A1 (2018).

[2] A. Serdyuchenko, V. Gorshelev, M. Weber, W. Chehade, and J. P. Burrows, "High spectral resolution ozone absorption cross-sections – Part 2: Temperature dependence," Atmos. Meas. Tech. **7**, 625–636 (2014).

[3] G. Xu, Z. Ke, C. Zhuang, Y. Li, R. Cai, Y. Yang, and X. Du, "Measurements and analysis of solar spectrum in near space," Energy Rep. **9**, 1764–1773 (2023), part of Special Issue: Selected papers from 2022 International Conference on Frontiers of Energy and Environment Engineering.

[4] H. T. Soares, J. R. S. Campos, L. C. Gomes-da Silva, F. A. Schaberle, J. M. Dabrowski, and L. G. Arnaut, "Pro-oxidant and antioxidant effects in photodynamic therapy: Cells recognise that not all exogenous ROS are alike," ChemBioChem **17**, 836–842 (2016).

[5] P. S. Maharjan and H. K. Bhattarai, "Singlet oxygen, photodynamic therapy, and mechanisms of cancer cell death," J. Oncol. **2022**, 7211485.

[6] P. R. Ogilby, "Singlet oxygen: There is indeed something new under the sun," Chem. Soc. Rev. **39**, 3181–3209 (2010).

[7] I. Adamovich, S. Agarwal, E. Ahedo, L. L. Alves, S. Baalrud, N. Babaeva, A. Bogaerts, A. Bourdon, P. J. Bruggeman, C. Canal, E. H. Choi, S. Coulombe, Z. Donkó, D. B. Graves, S. Hamaguchi, D. Hegemann, M. Hori, H.-H. Kim, G. M. W. Kroesen, M. J. Kushner, A. Laricchiuta, X. Li, T. E. Magin, S. Mededovic Thagard, V. Miller, A. B. Murphy, G. S. Oehrlein, N. Puac, R. M. Sankaran, S. Samukawa, M. Shiratani, M. Šimek, N. Tarasenko, K. Terashima, E. Thomas, Jr., J. Trieschmann, S. Tsikata, M. M. Turner, I. J. van der Walt, M. C. M. van de Sanden, and T. von Woedtke, "The 2022 plasma roadmap: Low temperature plasma science and technology," J. Phys. D: Appl. Phys. **55**, 373001 (2022).

[8] S. H. Ji, S. Yoo, S. Park, and M. J. Lee, "Biodegradation of low-density polyethylene by plasma-activated bacillus strain," Chemosphere **349**, 140763 (2024).

[9] Y. Itikawa, A. Ichimura, K. Onda, K. Sakimoto, K. Takayanagi, Y. Hatano, M. Hayashi, H. Nishimura, and S. Tsurubuchi, "Cross sections for collisions of electrons and photons with oxygen molecules," J. Phys. Chem. Ref. Data **18**, 23–42 (1989).

[10] Y. Itikawa, "Cross sections for electron collisions with oxygen molecules," J. Phys. Chem. Ref. Data **38**, 1–20 (2008).

[11] A. Zecca, G. P. Karwasz, and R. S. Brusa, "One century of experiments on electron-atom and molecule scattering: A critical review of integral cross-sections," Riv. Nuovo Cimento **19**, 1–146 (1996).

[12] M. J. Brunger and S. J. Buckman, "Electron–molecule scattering cross-sections. I. Experimental techniques and data for diatomic molecules," Phys. Rep. **357**, 215–458 (2002).

[13] K. Anzai, H. Kato, M. Hoshino, H. Tanaka, Y. Itikawa, L. Campbell, M. J. Brunger, S. J. Buckman, H. Cho, F. Blanco, G. Garcia, P. Limão-Vieira, and O. Ingólfsson, "Cross section data sets for electron collisions with H_2, O_2, CO, CO_2, N_2O and H_2O," Eur. Phys. J. D **66**, 36 (2012).

[14] G. P. Karwasz, R. S. Brusa, and A. Zecca, "Total scattering cross section," in *Interactions of Photons and Electrons with Molecules*, *Landolt-Börnstein - Group I Elementary Particles, Nuclei and Atom Vol. 17C* (Springer-Verlag, Berlin, Heidelberg, 2003), Chap. 6.1.

[15] S. J. Buckman, M. Brunger, and M. T. Elford, "Integral elastic cross sections," in *Interactions of Photons and Electrons with Molecules*, *Landolt-Börnstein - Group I Elementary Particles, Nuclei and Atoms Vol. 17C* (Springer-Verlag, Berlin, Heidelberg, 2003), Chap. 6.2.

[16] M. T. Elford, S. J. Buckman, and M. Brunger, "Elastic momentum transfer cross sections," *Interactions of Photons and Electrons with Molecules*, *Landolt-Börnstein - Group I Elementary Particles, Nuclei and Atoms, Vol. 17C* (Springer-Verlag, Berlin, Heidelberg, 2003), Chap. 6.3.

[17] B. G. Lindsay and M. A. Mangan, "Ionization" in *Interactions of Photons and Electrons with Molecules*, *Landolt-Börnstein - Group I Elementary Particles, Nuclei and Atoms Vol. 17C* (Springer-Verlag, Berlin, Heidelberg, 2003), Chap. 5.1.

[18] Y. Itikawa and A. Ichimura, "Cross sections for collisions of electrons and photons with atomic oxygen," J. Phys. Chem. Ref. Data **19**, 637–651 (1990).

[19] R. R. Laher and F. R. Gilmore, "Updated excitation and ionization cross sections for electron impact on atomic oxygen," J. Phys. Chem. Ref. Data **19**, 277–305 (1990).

[20] Y. Ni, H. Gu, J. Cui, X. Huang, and W. Li, "Monte Carlo calculation of electron energy degradation in a pure O_2 atmosphere," Astrophys. J. **977**, 5 (2024).

[21] M.-Y. Song, J.-S. Yoon, H. Cho, Y. Itikawa, G. P. Karwasz, V. Kokoouline, Y. Nakamura, and J. Tennyson, "Cross sections for electron collisions with methane," J. Phys. Chem. Ref. Data **44**, 023101 (2015).

[22] A. Salop and H. H. Nakano, "Total electron scattering cross sections in O_2 and Ne," Phys. Rev. A **2**, 127–131 (1970).

[23] K. P. Subramanian and V. Kumar, "Total electron scattering cross sections for molecular oxygen at low electron energies," J. Phys. B: At., Mol. Opt. Phys. **23**, 745 (1990).

[24] A. Zecca, R. S. Brusa, R. Grisenti, S. Oss, and C. Szmytkowski, "Electron-molecule absolute total cross sections: O_2 from 0.2 to 100 eV," J. Phys. B: At. Mol. Phys. **19**, 3353 (1986).

[25]C. Szmytkowski, K. Maciag, and G. Karwasz, "Absolute electron-scattering total cross section measurements for noble gas atoms and diatomic molecules," Phys. Scr. **54**, 271 (1996).
[26]I. Kanik, J. C. Nickel, and S. Trajmar, "Total electron scattering cross section measurements for Kr, O_2 and CO," J. Phys. B: At., Mol. Opt. Phys. **25**, 2189 (1992).
[27]K. P. Subramanian and V. Kumar, "Total electron scattering cross sections for argon, krypton and xenon at low electron energies," J. Phys. B: At. Mol. Phys. **20**, 5505 (1987).
[28]G. Sunshine, B. B. Aubrey, and B. Bederson, "Absolute measurements of total cross sections for the scattering of low-energy electrons by atomic and molecular oxygen," Phys. Rev. **154**, 1–8 (1967).
[29]G. Dalba, P. Fornasini, R. Grisenti, G. Ranieri, and A. Zecca, "Absolute total cross section measurements for intermediate energy electron scattering. II. N_2, O_2 and NO," J. Phys. B: At. Mol. Phys. **13**, 4695 (1980).
[30]M. S. Dababneh, Y.-F. Hsieh, W. E. Kauppila, C. K. Kwan, S. J. Smith, T. S. Stein, and M. N. Uddin, "Total-cross-section measurements for positron and electron scattering by O_2, CH_4, and SF_6," Phys. Rev. A **38**, 1207–1216 (1988).
[31]G. García, F. Blanco, and A. Williart, "Cross-sections for electron scattering by O_2 at intermediate and high energies, 0.1–10 keV," Chem. Phys. Lett. **335**, 227–233 (2001).
[32]T. Okumura, N. Kobayashi, A. Sayama, Y. Mori, H. Akasaka, K. Hosaka, T. Odagiri, M. Hoshino, and M. Kitajima, "Total cross-section for low-energy and very low-energy electron collisions with O_2," J. Phys. B: At., Mol. Opt. Phys. **52**, 035201 (2019).
[33]D. Field, G. Mrotzek, D. W. Knight, S. Lunt, and J. P. Ziesel, "High-resolution studies of electron scattering by molecular oxygen," J. Phys. B: At., Mol. Opt. Phys. **21**, 171 (1988).
[34]J. Randell, S. L. Lunt, G. Mrotzek, J. P. Ziesel, and D. Field, "Low energy electron scattering in H_2, N_2 and O_2," J. Phys. B: At., Mol. Opt. Phys. **27**, 2369 (1994).
[35]S. J. Buckman, D. T. Alle, M. J. Brennan, P. D. Burrow, J. C. Gibson, R. J. Gulley, M. Jacka, D. S. Newman, A. R. P. Rau, J. P. Sullivan, and K. W. Trantham, "Role of negative ion resonances in electron scattering from atoms and molecules," Aust. J. Phys. **52**, 473–491 (1999).
[36]T. W. Shyn and W. E. Sharp, "Angular distribution of electrons elastically scattered from O_2: 2.0-200-eV impact energy," Phys. Rev. A **26**, 1369–1372 (1982).
[37]I. Iga, L. Mu-Tao, J. C. Nogueira, and R. S. Barbieri, "Elastic differential cross section measurements for electron scattering from Ar and O_2 in the intermediate-energy range," J. Phys. B: At. Mol. Phys. **20**, 1095 (1987).
[38]J. P. Sullivan, J. C. Gibson, R. J. Gulley, and S. J. Buckman, "Low-energy electron scattering from O_2," J. Phys. B: At., Mol. Opt. Phys. **28**, 4319 (1995).
[39]M. A. Green, P. J. O. Teubner, B. Mojarrabi, and M. J. Brunger, "Resolution of a discrepancy between low-energy differential cross section measurements for elastic electron scattering from O_2," J. Phys. B: At., Mol. Opt. Phys. **30**, 1813 (1997).
[40]I. Linert, G. C. King, and M. Zubek, "Measurements of differential cross sections for elastic electron scattering in the backward direction by molecular oxygen," J. Phys. B: At., Mol. Opt. Phys. **37**, 4681 (2004).
[41]I. Kanik, S. Trajmar, and J. C. Nickel, "Total electron scattering and electronic state excitations cross sections for O_2, CO, and CH_4," J. Geophys. Res.: Planets **98**, 7447–7460 (1993).
[42]H. Daimon, S. Hayashi, T. Kondow, and K. Kuchitsu, "Measurements of differential cross sections of low-energy electrons elastically scattered by gas molecules. II. Scattering of 200–500 eV electrons by molecular oxygen," J. Phys. Soc. Jpn. **51**, 2641–2649 (1982).
[43]R. D. Hake and A. V. Phelps, "Momentum-transfer and inelastic-collision cross sections for electrons in O_2, CO, and CO_2," Phys. Rev. **158**, 70–84 (1967).
[44]Y. Itikawa, "Momentum-transfer cross sections for electron collisions with atoms and molecules," At. Data Nucl. Data Tables **14**, 1–10 (1974).
[45]B.-H. Jeon, "Determination of electron collision cross-sections for the oxygen molecule by using an electron swarm study," J. Korean Phys. Soc. **43**, 513–525 (2003).
[46]H. Tanaka, M. J. Brunger, L. Campbell, H. Kato, M. Hoshino, and A. Rau, "Scaled plane-wave Born cross sections for atoms and molecules," Rev. Mod. Phys. **88**, 025004 (2016).
[47]L. L. Alves, P. Coche, M. A. Ridenti, and V. Guerra, "Electron scattering cross sections for the modelling of oxygen-containing plasmas," Eur. Phys. J. D **70**, 124 (2016).
[48]E. Gerjuoy and S. Stein, "Rotational excitation by slow electrons," Phys. Rev. **97**, 1671 (1955).
[49]K. K. Irikura, "Experimental vibrational zero-point energies: Diatomic molecules," J. Phys. Chem. Ref. Data **36**, 389–397 (2007).
[50]V. W. Couling and S. S. Ntombela, "The electric quadrupole moment of O_2," Chem. Phys. Lett. **614**, 41–44 (2014).
[51]S. Harrison, J. Tennyson, and A. Faure, "Calculated electron impact spin-coupled rotational cross sections for $^{2S+1}\Sigma^+$ linear molecules: CN as an example," J. Phys. B: At., Mol. Opt. Phys. **45**, 175202 (2012).
[52]A. Faure and J. Tennyson, "Electron-impact rotational excitation of linear molecular ions," Mon. Not. R. Astron. Soc. **325**, 443–448 (2001).
[53]M. Allan, "Measurement of absolute differential cross sections for vibrational excitation of O_2 by electron impact," J. Phys. B: At., Mol. Opt. Phys. **28**, 5163 (1995).
[54]V. Laporta, R. Celiberto, and J. Tennyson, "Resonant vibrational-excitation cross sections and rate constants for low-energy electron scattering by molecular oxygen," Plasma Sources Sci. Technol. **22**, 025001 (2013).
[55]T. W. Shyn and C. J. Sweeney, "Vibrational-excitation cross sections of molecular oxygen by electron impact," Phys. Rev. A **48**, 1214 (1993).
[56]C. J. Noble and P. G. Burke, "*R*-matrix calculations of low-energy electron scattering by oxygen molecules," Phys. Rev. Lett. **68**, 2011–2014 (1992).
[57]F. Linder and H. Schmidt, "Experimental study of low energy e-O_2 collision processes," Z. Naturforsch. **26**, 1617–1625 (1971).
[58]S. F. Wong, M. J. W. Boness, and G. J. Schulz, "Vibrational excitation of O_2 by electron impact above 4 eV," Phys. Rev. Lett. **31**, 969 (1973).
[59]C. J. Noble, K. Higgins, G. Wöste, P. Duddy, P. G. Burke, P. J. O. Teubner, A. G. Middleton, and M. J. Brunger, "Resonant mechanisms in the vibrational excitation of ground state O_2," Phys. Rev. Lett. **76**, 3534 (1996).
[60]M. J. Brunger, A. G. Middleton, and P. J. O. Teubner, "Differential cross sections for rovibrational $v' = 0 \rightarrow 1, 2, 3, 4$ excitation of the electronic ground state of O_2 by electron impact," Phys. Rev. A **57**, 208 (1998).
[61]I. Linert and M. Zubek, "Differential cross sections for electron impact vibrational excitation of molecular oxygen in the angular range 15°–180°," J. Phys. B: At., Mol. Opt. Phys. **39**, 4087 (2006).
[62]K. Higgins, C. J. Gillan, P. G. Burke, and C. J. Noble, "Low-energy electron scattering by oxygen molecules. II. Vibrational excitation," J. Phys. B: At., Mol. Opt. Phys. **28**, 3391 (1995).
[63]V. Alt and K. Houfek, "Resonant collisions of electrons with O_2 via the lowest-lying $^2\Pi_g$ state of O_2^-," Phys. Rev. A **103**, 032829 (2021).
[64]J. D. Gorfinkiel, A. Faure, S. Taioli, C. Piccarreta, G. Halmová, and J. Tennyson, "Electron-molecule collisions at low and intermediate energies using the R-matrix method," Eur. Phys. J. D **35**, 231–237 (2005).
[65]D. A. Long, D. K. Havey, M. Okumura, C. E. Miller, and J. T. Hodges, "O_2 A-band line parameters to support atmospheric remote sensing," J. Quant. Spectrosc. Radiat. Transfer **111**, 2021–2036 (2010).
[66]K. Bielska, J. Domysławska, S. Wójtewicz, A. Balashov, M. Słowiński, M. Piwiński, A. Cygan, R. Ciuryło, and D. Lisak, "Simultaneous observation of speed dependence and Dicke narrowing for self-perturbed P-branch lines of O_2 B band," J. Quant. Spectrosc. Radiat. Transfer **276**, 107927 (2021).
[67]C. E. Brion, K. H. Tan, M. J. van der Wiel, and P. E. van der Leeuw, "Dipole oscillator strengths for the photoabsorption, photoionization and fragmentation of molecular oxygen," J. Electron. Spectrosc. Relat. Phenom. **17**, 101 (1979).
[68]W.-Q. Xu, J.-M. Sun, Y.-Y. Wang, and L.-F. Zhu, "Generalized oscillator strengths and integral cross sections for the valence-shell excitations of oxygen studied by fast electron impact," Phys. Rev. A **82**, 042716 (2010).
[69]Y.-W. Liu, Y.-G. Peng, T. Xiong, S.-X. Wang, X.-C. Huang, Y. Wu, and L.-F. Zhu, "Generalized oscillator strengths of the low-lying valence-shell excitations of N_2, O_2, and C_2H_2 studied by fast electron and inelastic X-ray scattering," J. Chem. Phys. **150**, 094302 (2019).
[70]D. Hayashi and K. Kadota, "Efficient production of O^- by dissociative attachment of slow electrons to highly excited metastable oxygen molecules," Jpn. J. Appl. Phys. **38**, 225 (1999).

[71]J. Shi and J. R. Barker, "Odd oxygen formation in the laser irradiation of O_2 at 248 nm: Evidence for reactions of O_2 in the Herzberg states with ground state O_2," J. Geophys. Res.: Atmos. **97**, 13039–13050 (1992).
[72]S. M. L. Melo, H. Takahashi, B. R. Clemesha, and J. Stegman, "The O_2 Herzberg I bands in the equatorial nightglow," J. Atmos. Solar-Terr. Phys. **59**, 295–303 (1997).
[73]W. F. Chan, G. Cooper, and C. E. Brion, "Absolute optical oscillator strengths for the photoabsorption of molecular oxygen (5–30 eV) at high resolution," Chem. Phys. **170**, 99 (1993).
[74]T. G. Slanger, P. C. Cosby, and D. L. Huestis, "A new O_2 band system: The $c^1\Sigma_u^- - b^1\Sigma_g^+$ transition in the terrestrial nightglow," J. Geophys. Res.: Space Phys. **108**, 1089 (2003).
[75]T. W. Shyn and C. J. Sweeney, "Differential electronic-excitation cross sections of molecular oxygen by electron impact: The $a\ ^1\Delta_g$ and $^1\Sigma_g^+$ states," Phys. Rev. A **47**, 1006 (1993).
[76]D. Teillet-Billy, L. Malegat, and J. P. Gauyacq, "Electronic excitation as a resonant process: e^-O_2 collisions," J. Phys. B: At. Mol. Phys. **20**, 3201 (1987).
[77]T. W. Shyn, C. J. Sweeney, A. Grafe, and W. E. Sharp, "Absolute differential cross sections for the excitation of molecular oxygen by electron impact: Decomposition of the Schumann-Runge continuum," Phys. Rev. A **50**, 4794 (1994).
[78]L. E. Machado, E. M. S. Ribeiro, M.-T. Lee, M. M. Fujimoto, and L. M. Brescansin, "Cross sections and polarization fractions for elastic $e^- - O_2$ collisions," Phys. Rev. A **60**, 1199 (1999).
[79]A. G. Middleton, M. J. Brunger, P. J. O. Teubner, M. W. B. Anderson, C. J. Noble, G. Woste, K. Blum, P. G. Burke, and C. Fullerton, "Differential cross sections for the electron impact excitation of the $a^1\Delta_g$ and $b^1\Sigma_g^+$ electronic states of O_2," J. Phys. B: At., Mol. Opt. Phys. **27**, 4057 (1994).
[80]M. Tashiro, K. Morokuma, and J. Tennyson, "*R*-matrix calculation of electron collisions with electronically excited O_2 molecules," Phys. Rev. A **73**, 052707 (2006).
[81]J. Singh and K. L. Baluja, "Electron-impact study of the O_2 molecule using the *R*-matrix method," Phys. Rev. A **90**, 022714 (2014).
[82]C. Huang, H. Zhang, and X. Cheng, "R-matrix calculation of electron collisions with molecular oxygen in its electronically excited states," J. Phys. Chem. A **126**, 2061–2074 (2022).
[83]C. J. Gillan, O. Nagy, P. G. Burke, L. A. Morgan, and C. J. Noble, "Electron scattering by nitrogen molecules," J. Phys. B: At. Mol. Phys. **20**, 4585 (1987).
[84]B. Cooper, M. Tudorovskaya, S. Mohr, A. O'Hare, M. Hanicinec, A. Dzarasova, J. Gorfinkiel, J. Benda, Z. Mašín, A. Al-Refaie, P. J. Knowles, and J. Tennyson, "Quantemol electron collisions (QEC): An enhanced expert system for performing electron molecule collision calculations using the R-matrix method," Atoms **7**, 97 (2019).
[85]J. P. Doering, "Absolute differential and integral electron excitation cross sections for the O_2 (a^1 g ← x^3 g) transition," J. Geophys. Res.: Space Phys. **97**, 12267–12270 (1992).
[86]D. Teillet-Billy, L. Malegat, J. P. Gauyacq, R. Abouaf, and C. Benoit, "Electronic excitation to the O_2 ($\ldots\pi_u^3\pi_g^3$) states in e^-O_2 collisions," J. Phys. B: At., Mol. Opt. Phys. **22**, 1095 (1989).
[87]R. I. Hall and S. Trajmar, "Scattering of 4.5 eV electrons by ground ($X^3\Sigma_g^-$) state and metastable ($a^1\Delta_g$) oxygen molecules," J. Phys. B: Mol. Phys. **8**, L293 (1975).
[88]P. Wang, S. Gong, and Y. Mo, "Bond dissociation energy of O_2 measured by fully state-to-state resolved threshold fragment yield spectra," J. Chem. Phys. **160**, 164302 (2024).
[89]P. C. Cosby, "Electron-impact dissociation of oxygen," J. Chem. Phys. **98**, 9560–9569 (1993).
[90]P. C. Cosby, "Electron-impact dissociation of nitrogen," J. Chem. Phys. **98**, 9544–9553 (1993).
[91]M.-Y. Song, H. Cho, G. P. Karwasz, V. Kokoouline, and J. Tennyson, "Cross sections for electron collisions with N_2, N_2^+, and N_2^*," J. Phys. Chem. Ref. Data **52**, 023104 (2023).
[92]L. R. LeClair and J. W. McConkey, "Selective detection of $O(^1S)$ following electron impact dissociation of O_2 and N_2O using a XeO* conversion technique," J. Chem. Phys. **99**, 4566–4577 (1993).
[93]J. T. Tate and P. T. Smith, "The efficiencies of ionization and ionization potentials of various gases under electron impact," Phys. Rev. **39**, 270 (1932).
[94]D. Rapp and P. Englander-Golden, "Total cross sections for ionization and attachment in gases by electron impact. I. Positive ionization," J. Chem. Phys. **43**, 1464–1479 (1965).
[95]T. D. Märk, "Cross section for single and double ionization of N_2 and O_2 molecules by electron impact from threshold up to 170 eV," J. Chem. Phys. **63**, 3731–3736 (1975).
[96]E. Krishnakumar and S. K. Srivastava, "Cross-sections for electron impact ionization of O_2," Int. J. Mass Spectrom. Ion Process. **113**, 1–12 (1992).
[97]C. Tian and C. R. Vidal, "Electron impact ionization of N_2 and O_2: Contributions from different dissociation channels of multiply ionized molecules," J. Phys. B: At., Mol. Opt. Phys. **31**, 5369 (1998).
[98]H. C. Straub, P. Renault, B. G. Lindsay, K. A. Smith, and R. F. Stebbings, "Absolute partial cross sections for electron-impact ionization of H_2, N_2, and O_2 from threshold to 1000 eV," Phys. Rev. A **54**, 2146–2153 (1996).
[99]J. N. Bull, J. W. L. Lee, and C. Vallance, "Electron ionization dynamics of N_2 and O_2 molecules: Velocity-map imaging," Phys. Rev. A **91**, 022704 (2015).
[100]L. Sigaud, N. Ferreira, and E. C. Montenegro, "Absolute cross sections for O_2 dication production by electron impact," J. Chem. Phys. **139**, 024302 (2013).
[101]S. Jia, J. Zhou, X. Wang, X. Xue, X. Hao, Q. Zeng, Y. Zhao, Z. Xu, A. Dorn, and X. Ren, "Cold-target electron-ion-coincidence momentum-spectroscopy study of electron-impact single and double ionization of N_2 and O_2 molecules," Phys. Rev. A **107**, 032819 (2023).
[102]J. P. Doering and J. Yang, "Direct experimental measurement of electron impact ionization-excitation branching ratios 4. Branching ratios and cross sections for O_2^+ at 100 eV," J. Geophys. Res.: Space Phys. **102**, 9691–9696 (1997).
[103]D. C. Frost and C. A. McDowell, "The ionization and dissociation of oxygen by electron impact," J. Am. Chem. Soc. **80**, 6183–6187 (1958).
[104]C. E. Brion, "Ionization of oxygen by monoenergetic electrons," J. Chem. Phys. **40**, 2995 (1964).
[105]M. Fu, S. Pan, L. Zhao, and G. Frenking, "Bonding analysis of the shortest bond between two atoms heavier than hydrogen and helium: O_2^+," J. Phys. Chem. A **124**, 1087 (2020).
[106]H. Cho and S. H. Lee, "Double ionization of O_2 by electron impact," Phys. Rev. A **48**, 2468–2470 (1993).
[107]H. Cho and J.-H. Lee, "Angular distributions of O^+ from O_2^{2+} produced by electron impact on O_2," Phys. Rev. A **54**, 3665 (1996).
[108]R. A. Lomsadze, M. R. Gochitashvili, R. Y. Kezerashvili, and M. Schulz, "Electron-impact ionization and ionic fragmentation of O_2 from threshold to 120 eV energy range," Int. J. Mod. Phys. B **35**, 2150104 (2021).
[109]B. Evans, J. S. Chang, A. W. Yau, R. W. Nicholls, and R. M. Hobson, "Studies of the electron-impact ionization cross section of vibrationally excited oxygen employing a shock-heated molecular beam," Phys. Rev. A **38**, 2782–2788 (1988).
[110]D. Rapp and D. D. Briglia, "Total cross sections for ionization and attachment in gases by electron impact. II. Negative-ion formation," J. Chem. Phys. **43**, 1480–1489 (1965).
[111]L. G. Christophorou, R. N. Compton, G. S. Hurst, and P. W. Reinhardt, "Determination of electron-capture cross sections with swarm-beam techniques," J. Chem. Phys. **43**, 4273–4281 (1965).
[112]V. Laporta, R. Celiberto, and J. Tennyson, "Dissociative electron attachment and electron-impact resonant dissociation of vibrationally excited O_2 molecules," Phys. Rev. A **91**, 012701 (2015).
[113]R. J. Van Brunt and L. J. Kieffer, "Angular distribution of O^- from dissociative electron attachment to O_2," Phys. Rev. A **2**, 1899–1905 (1970).
[114]V. S. Prabhudesai, D. Nandi, and E. Krishnakumar, "On the presence of the $^4\Sigma_u^-$ resonance in dissociative electron attachment to O_2," J. Phys. B: At., Mol. Opt. Phys. **39**, L277 (2006).
[115]W. R. Henderson, W. L. Fite, and R. T. Brackmann, "Dissociative attachment of electrons to hot oxygen," Phys. Rev. **183**, 157–166 (1969).
[116]P. D. Burrow, "Dissociative attachment from the $O_2(a^1\Delta_g)$ state," J. Chem. Phys. **59**, 4922–4931 (1973).

[117]Y. Itikawa, "Electron attachment cross sections," in *Interactions of Photons and Electrons with Molecules*, *Landolt-Börnstein - Group I Elementary Particles, Nuclei and Atoms Vol. 17C* (Springer-Verlag, Berlin, Heidelberg, 2003), Chap. 5.2.
[118]S. K. R. Miller and B. A. Banks, "Atomic oxygen environments, effects and mitigation," in Applied Space Environments Conference, Los Angeles, 2019.
[119]X. Wu, J. Cui, S. Wu, H. Gu, Y. Cao, W. Liang, and S. Liao, "Modeling the structure of the dayside Venusian ionosphere: Impacts of protonation and Coulomb interaction," Astron. Astrophys. **685**, A160 (2024).
[120]A. T. Archibald, J. L. Neu, Y. F. Elshorbany, O. R. Cooper, P. J. Young, H. Akiyoshi, R. A. Cox, M. Coyle, R. G. Derwent, M. Deushi, A. Finco, G. J. Frost, I. E. Galbally, G. Gerosa, C. Granier, P. T. Griffiths, R. Hossaini, L. Hu, P. Jöckel, B. Josse, M. Y. Lin, M. Mertens, O. Morgenstern, M. Naja, V. Naik, S. Oltmans, D. A. Plummer, L. E. Revell, A. Saiz-Lopez, P. Saxena, Y. M. Shin, I. Shahid, D. Shallcross, S. Tilmes, T. Trickl, T. J. Wallington, T. Wang, H. M. Worden, and G. Zeng, "Tropospheric ozone assessment report: A critical review of changes in the tropospheric ozone burden and budget from 1850 to 2100," Elementa: Sci. Anthropocene **8**, 034 (2020).
[121]E. Spanswick, J. Liang, J. Houghton, D. Chaddock, E. Donovan, B. Gallardo-Lacourt, C. Keenan, J. Rosehart, Y. Nishimura, D. Hampton, and M. Gillies, "Association of structured continuum emission with dynamic aurora," Nat. Commun. **15**, 10802 (2024).
[122]J. F. Williams and L. J. Allen, "Low-energy elastic scattering of electrons from atomic oxygen," J. Phys. B: At., Mol. Opt. Phys. **22**, 3529 (1989).
[123]S. S. Tayal and O. Zatsarinny, "*B*-spline *R*-matrix-with-pseudostates approach for excitation and ionization of atomic oxygen by electron collisions," Phys. Rev. A **94**, 042707 (2016).
[124]F. Blanco and G. Garćia (private communication, 2025); A description of the method can be found in K. R. Hamilton *et al.*, J. Phys. Chem. Ref. Data **50**, 013101 (2021).
[125]O. Zatsarinny and S. S. Tayal, "Low-energy electron collisions with atomic oxygen: *R*-matrix calculation with non-orthogonal orbitals," J. Phys. B: At., Mol. Opt. Phys. **34**, 1299 (2001).
[126]M. Plummer, C. J. Noble, and M. L. Dourneuf, "Low-energy behaviour of e–O scattering calculations," J. Phys. B: At., Mol. Opt. Phys. **37**, 2979 (2004).
[127]P. V. Johnson, I. Kanik, M. A. Khakoo, J. W. McConkey, and S. S. Tayal, "Low-energy differential and integral electron-impact cross sections for the $2s^2 2p^4\ ^3P \rightarrow 2p^3 3s\ ^3S^o$ excitation in atomic oxygen," J. Phys. B: At., Mol. Opt. Phys. **36**, 4289 (2003).
[128]S. O. Vaughan and J. P. Doering, "Absolute experimental differential and integral electron excitation cross sections for atomic oxygen: 4. The ($^3P \rightarrow 3s''\ ^3P^o$), ($^3P \rightarrow 2s2p^5\ ^3P^o$), ($^3P \rightarrow 4d'\ ^3P^o$), autoionizing transitions (878, 792, and 770 Å) and five members of the ($^3P \rightarrow nd\ ^3D^o$) Rydberg series (1027 Å)," J. Geophys. Res.: Space Phys. **93**, 289–293 (1988).
[129]I. Kanik, P. V. Johnson, M. B. Das, M. A. Khakoo, and S. S. Tayal, "Electron-impact studies of atomic oxygen: I. Differential and integral cross sections; experiment and theory," J. Phys. B: At., Mol. Opt. Phys. **34**, 2647 (2001).
[130]S. S. Tayal, "Accurate cross sections for excitation of resonance transitions in atomic oxygen," J. Geophys. Res.: Space Phys. **109** (2004).
[131]Y. Wang and Y. Zhou, "The effects of discrete and continuum states on the $2p^4 {}^3P \rightarrow 2p^3 3s\ ^3S^o$ transition of atomic oxygen by electron impact," J. Phys. B: At., Mol. Opt. Phys. **39**, 3009 (2006).
[132]J. P. Doering, "Absolute differential and integral electron excitation cross sections for atomic oxygen: 9. Improved cross section for the $^3P \rightarrow {}^1D$ transition from 4.0 to 30 eV," J. Geophys. Res.: Space Phys. **97**, 19531–19534 (1992).
[133]T. W. Shyn and W. E. Sharp, "Differential excitation cross section of atomic oxygen by electron impact: ($^3P \rightarrow {}^1D$ transition)," J. Geophys. Res.: Space Phys. **91**, 1691–1697 (1986).
[134]J. P. Doering and E. E. Gulcicek, "Absolute differential and integral electron excitation cross sections for atomic oxygen 7. The $^3P \rightarrow {}^1D$ and $^3P \rightarrow {}^1S$ transitions from 4.0 to 30 eV," J. Geophys. Res.: Space Phys. **94**, 1541–1546 (1989).
[135]J. P. Doering and E. E. Gulcicek, "Absolute differential and integral electron excitation cross sections for atomic oxygen 8. The $^3P \rightarrow {}^5S$ transition (1356 Å) from 13.9 to 30 eV," J. Geophys. Res.: Space Phys. **94**, 2733–2736 (1989).
[136]E. Brook, M. F. A. Harrison, and A. C. H. Smith, "Measurements of the electron impact ionisation cross sections of He, C, O and N atoms," J. Phys. B: At. Mol. Phys. **11**, 3115 (1978).
[137]Y.-K. Kim and J.-P. Desclaux, "Ionization of carbon, nitrogen, and oxygen by electron impact," Phys. Rev. A **66**, 012708 (2002).
[138]W. R. Thompson, M. B. Shah, and H. B. Gilbody, "Single and double ionization of atomic oxygen by electron impact," J. Phys. B: At., Mol. Opt. Phys. **28**, 1321 (1995).
[139]E. C. Zipf, "The ionization of atomic oxygen by electron impact," Planet. Space Sci. **33**, 1303–1307 (1985).
[140]J. H. Waite, Jr., T. K. Greathouse, S. R. Carberry Mogan, A. H. Sulaiman, P. Valek, F. Allegrini, R. W. Ebert, G. R. Gladstone, W. S. Kurth, J. E. P. Connerney, G. Clark, F. Bagenal, S. Duling, N. Romanelli, S. Bolton, A. Vorburger, C. Paranicas, P. Kollmann, B. Mauk, C. Hansen, D. Buccino, R. E. Johnson, R. J. Wilson, and B. Teolis, "Magnetospheric-ionospheric-atmospheric implications from the Juno flyby of Ganymede," J. Geophys. Res.: Planets **129**, e2023JE007859 (2024).